Coordinated Frequency Control for Isolated Power Systems with High Penetration of DFIG-based Wind Power

Xin Ding, Wei Lin, *Fellow*, *IEEE*, Jian Xu, *Senior Member*, *IEEE*, *Senior Member*, *CSEE*, Yuanzhang Sun, *Senior Member*, *IEEE*, Liangzhong Yao, *Fellow*, *IEEE*, and Beilin Mao

***Abstract*—This paper proposes a coordinated frequency control scheme for emergency frequency regulation of isolated power systems with a high penetration of wind power. The proposed frequency control strategy is based on the novel nonlinear regulator theory, which takes advantage of nonlinearity of doubly fed induction generators (DFIGs) and generators to regulate the frequency of the power system. Frequency deviations and power imbalances are used to design nonlinear feedback controllers that achieve the reserve power distribution between generators and DFIGs, in various wind speed scenarios. The effectiveness and dynamic performance of the proposed nonlinear coordinated frequency control method are validated through simulations in an actual isolated power grid.**

***Index Terms*—Frequency control, isolated power systems, nonlinear feedback, nonlinear regulator theory, wind power.**

NOMENCLATURE

$i_{\rm r}$, i_g, i_t	Current at rotor side control, grid side control and terminal of DFIG.
$u_{\rm dc}$, u_t	Voltage at DC link and terminal of DFIG.
$u_{\rm r\_ref}$, $u_{\rm g\_ref}$	Voltage reference on rotor side control and grid side control of DFIG.
$P_{\rm wm}$	Mechanical output power of DFIG.
$C_{\rm p}(\lambda,\theta)$	Power coefficient of DFIG.
λ	Tip speed ratio of DFIG.
θ	Pitch angle of DFIG.
ρ	Air density.
$\boldsymbol{A}$	Blade swept area of DFIG.
$\boldsymbol{R}$	Blade radius.
$V_{\rm w}$	Wind speed.
$V_{\rm rate}$	Rated wind speed.
$V_{\rm RSC-lim}$	Wind speed limit for RSC.
$\omega_{\rm r}$	Turbine rotor speed.
$\omega_{\rm lim}$	Maximum of rotor speed.
M, D	Equivalent inertia constant and load damping.
Δf	Frequency deviation.
ΔP_D	Active power disturbance.
R_i	Droop control coefficient of generator i.
$\Delta X_{{\rm G}i}$	Valve position deviation of generator i.
$T_{{\rm RH}i}$	Time constant of reheater i.
$\Delta P_{{\rm RH}i}$	Output power deviation of reheater i.
$K_{\rm HPi}$	Fraction of turbine power generated by high pressure unit of generator i.
$\Delta P_{{\rm G}i}$	Output power deviation of steam turbine i.
$T_{{\rm G}i}$, $T_{\rm Ti}$	Time constants of speed governor i and steam turbine i.
$P_{\rm grefi}$	Control input of generator i.
$P_{\rm wrefj}$	Control input of DFIG j.
$\Delta P_{{\rm we}j}$	Electromagnetic power deviation of DFIG j.
$\boldsymbol{x}$, $\tilde{\boldsymbol{x}}$	System state.
$\boldsymbol{y}$, $\tilde{\boldsymbol{y}}$	System output.
$\boldsymbol{u}$, $\tilde{\boldsymbol{u}}$	Control input.
$\boldsymbol{w}$, $\tilde{\boldsymbol{w}}$	External signal.
$\boldsymbol{e}$	Error signal.
$\boldsymbol{\pi}(\boldsymbol{w})$, $\boldsymbol{c}(\boldsymbol{w})$	Solution of regulator equations.
$\boldsymbol{K}$, $\boldsymbol{K}_s$	Feedback gain matrices.
k_{gi}, k_{wj}, $\tilde{k}_{gi}$, $\tilde{k}_{wj}$	Feedback gain of generator i and DFIG j.
$k_{\rm pd}$, $\tilde{k}_{\rm pd}$	Power distribution coefficient between generators and DFIGs.
k_{gdi}, $\tilde{k}_{gdi}$	Reserve power distribution coefficient for generator i.

Manuscript received November 8, 2021; revised January 17, 2022; accepted February 7, 2022. Date of online publication May 6, 2022; date of current version November 22, 2023. This work was supported by National Natural Science Foundation of China (U2066601).

X. Ding, J. Xu (corresponding author, email: xujian@whu.edu.cn), Y. Z. Sun, L. Z. Yao and B. L. Mao are with the School of Electrical Engineering and Automation, Wuhan University, Wuhan 430072, China.

W. Lin is with the Department of Electrical Engineering and Computer Science, Case Western Reserve University, Cleveland, OH 44106 USA.

DOI: 10.17775/CSEEJPES.2021.08320

I. INTRODUCTION

DUE to the growing demand of the power load and the dwindling of fossil fuels, renewable energy, such as wind power, has been widely used in the past decade. As a result, installed wind power capacity has increased rapidly. By the end of 2020, the installed wind power capacity in China has already reached 281.53 GW, while the total electricity generated from wind in 2020 reached 466.5 TWh, representing 34.6% and 15.1% increases, respectively, much higher than in 2019 [1]. To promote the utilization of wind energy and improve the economic benefit of industrial production, isolated power systems have been constructed as an effective solution in many countries, including China, Greece Denmark and Israel [2]–[5], to name just a few. However, due to the simple structure and disconnection from the utility grid,

the system inertia of the isolated power system is much smaller than that of the large power grid. Moreover, high penetration of wind power integrated in the isolated power grid may further deteriorate the system's stability [6]. For this reason, frequency control is one of the major issues in the operation of isolated power systems [7]. On one hand, high penetration of wind power would decrease conventional power plants' generation, which might deteriorate the system's fast frequency regulation ability [8]. On the other hand, wind power fluctuation would introduce large power imbalances and bring reserve management issues of conventional plants, which have been a technical concern to the operators of isolated power systems [9].

This paper studies extreme working scenarios (e.g., short circuit faults) of the isolated power system with high wind power penetration. Compared with wind power fluctuation, such emergencies in the isolated power system are more likely to lead to catastrophic results in frequency stability, as a result of lacking sufficient primary frequency reserve capacity. The frequency may collapse instantly when large active power imbalance occurs between generation and load demand [10].

For conventional large-scale power systems, the common approaches include active power regulation of governors [11] and load shedding strategies [12]. They are, however, not particularly practical to ensure reliable and economical operation for an isolated power grid. To reduce the impact on frequency stability of the isolated power system, a common solution is to use the energy storage system (ESS) to provide fast frequency response [13], [14]. However, the ESS method is not cost effective and it is neither practical nor economical to install large-capacity ESSs in an isolated power system. To address the emergency frequency control problem in the situation of high proportion of wind power, we focus, in this paper, on how to regulate thermal governors and wind turbines in a coordinated manner.

In the existing literature, several researchers have investigated the problem of how to maintain system frequency within a normal range by controlling the wind turbine. In [15], the active and reactive power output of DFIG wind turbines can be controlled by using vector control techniques. [16] pointed out that DFIGs have a potential in providing frequency support if they work in a deloaded mode. Reference [17] made an assessment about financial benefits and operational costs of frequency support from wind farms in the future Great Britain power system. In [18], the authors studied the inertia and frequency responses of wind farms and proposed a governor-like droop control scheme for wind turbines.

The coordination between the wind turbines and thermal generators needs to be taken into consideration when designing frequency control methods [19]. The coordinated frequency regulation methods have been studied by many researchers. In [20], a generic frequency controller including the transient inertial response and the permanent droop-based response was proposed to provide primary frequency reserve in the actual power system of Rhodes Island, Greece. In [21], the authors proposed a variable coefficient combined virtual inertia and primary frequency control strategy for DFIGs and diesel generators in a microgrid. A coordinated active power control strategy for wind turbines is designed in [22] to improve the performance of automatic generation control (AGC) by setting power command signals. These control methods basically applied PI and PID controllers to achieve control objectives. However, the parameters of the PI and PID controller are not easily determined, especially under the variable wind speed scenarios, likely resulting in poor dynamic performance. In addition, the PI and PID controllers are not effective in dealing with inherent nonlinearity of DFIGs. For the isolated power system with high wind power penetration, how to compensate the affect caused by the strong nonlinearity of DFIGs is a critical issue that must be considered to achieve effective frequency regulation.

Several researchers have applied model predictive control (MPC) instead of the PID control to improve the dynamic performance. [23] proposed an MPC-based coordinated control strategy of wind turbine pitch angle and plug-in hybrid electric vehicles for load frequency control of microgrids. In [24], the authors presented a hierarchical distributed MPC strategy to realize coordination power dispatch in a standalone wind-solar-battery hybrid power system. In [25], a coordinated energy management based on distributed MPC of heterogeneous energy resources was given to optimize the performance of microgrids and reduce the operation costs. Although MPC controllers are capable of achieving satisfactory performance, they rely heavily on the online optimization algorithms whose computational burden significantly increases when the dimension of the power system increases.

To avoid the complexity of optimization algorithms, we aim in this paper at developing a linearization-based nonlinear regulator method for the coordinated frequency regulation of an isolated power system with high wind power penetration, which takes the strong nonlinearity of wind turbine into account. The linear regulator theory has been applied for the controller design, leading to satisfactory dynamic performance [26], [27]. In [26], the authors proposed a generator excitation voltage control scheme based on the linear regulator theory for the emergency frequency regulation in an isolated power system. A demand side control based on the output regulation theory has been more recently developed in [27], for smoothing the short-term power fluctuation in industrial microgrids. In this research, based on the nonlinear regulator theory, a coordinated frequency control method is derived from the load frequency control model of the isolated power system, which is used to restore the frequency to a normal value when a large active power imbalance occurs in the isolated power grid with high wind power penetration.

The main contributions of this paper are summarized as follows:

1) A coordinated frequency control model combining generators and DFIGs is proposed for the isolated power system, which is applicable to scenarios under different wind speeds.

2) The problem of coordinated frequency control is formulated as a nonlinear regulator problem. Using the regulator theory, frequency controllers are designed in this paper. The proposed control scheme uses only the signals of frequency deviation and power imbalance. It is effective in increasing fast frequency regulating capability of the isolated power system

and restoring the frequency to a normal value. In addition, the proposed frequency controller is also robust against the wind speed fluctuation.

The remainder of this paper is organized as follows. Section II describes frequency control problems in an actual island power system with high penetration of wind power. The frequency control model of the power system is presented in Section III. Section IV introduces a coordinated frequency control method based on the nonlinear regulator theory and its design procedure. The simulation results conducted on the actual isolated power system are presented in Section V. Conclusions are given in Section VI.

II. Frequency Control Issues of The Actual Isolated Power System With Wind Power

In this paper, an isolated industrial power system, which has been constructed for aluminum production in Inner Mongolia, China [8]–[10], is considered as a case study. Due to the rich wind energy and coal resources in Inner Mongolia, the local government plans to develop the electrolytic aluminum industry. The electric power and energy balance of the system and the economic efficiency have been analyzed in [28]. Based on the techno-economical assessment, constructing the isolated power system for all electrolytic aluminum production is feasible and profitable. Thus, a wind-coal supplied isolated power system consisting of 1800 MW thermal generators, 800 MW wind turbines, 1390 MW electrolytic aluminum loads and 40 MW heating loads has been constructed as shown in Fig. 1. The installed capacity and power demand of thermal generators, wind farms and loads are listed in Tables I and Table II, respectively.

There are eight coal-fired generators with total capacity of 1800 MW and two 400 MW DFIG-based wind farms. In terms of installed capacity, the penetration of wind power reaches to 30.8%.

TABLE I
Installed Capacity of Thermal Generators and Wind Farms

G1/G2	G3/G4	G5/G6	G7/G8	W1/W2
100 MW	150 MW	300 MW	350 MW	400 MW

TABLE II
Power Demand of Electrolytic Aluminum Loads and Heating Loads

Aluminum Load 1	Aluminum Load 2	Aluminum Load 3	Heating Load 1	Heating Load 2	Heating Load 3
330 MW	420 MW	640 MW	20 MW	10 MW	10 MW

The system frequency response (SFR) model in [29] is adopted to estimate the frequency behaviour of the isolated power system in response to power disturbances, such as wind power fluctuation, thermal generator tripping or load shedding. The block diagram of the SFR is shown in Fig. 2 and the equivalent parameters of the isolated power system in the SFR model are listed in Table III. The identification process of the equivalent parameters has been introduced in detail in [10]. P_{SP}, P_m, P_e are the incremental power set point, turbine mechanical power and generator electrical load power, respectively. $\Delta\omega$ is the incremental speed. F_H, T_R are the fractions of total power generated by the HP turbine and the reheat time constant. K_m is the mechanical power gain factor. H, D, and R are the inertia constant, damping factor and droop control coefficient, respectively.

A typical working situation for generators and wind farms is shown in Table IV. Per the requirements of power system security, such as the "$N-1$" rule, power imbalance between generation and demand may occur in some extreme scenarios. For example, if one of thermal generators G5 is out of service

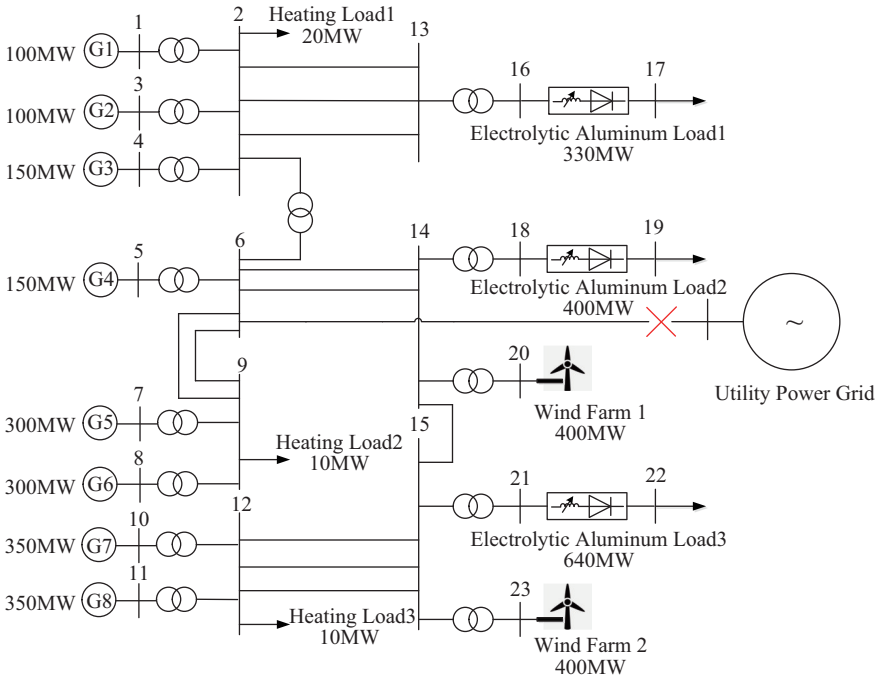

Fig. 1. The structure of an actual isolated power system.

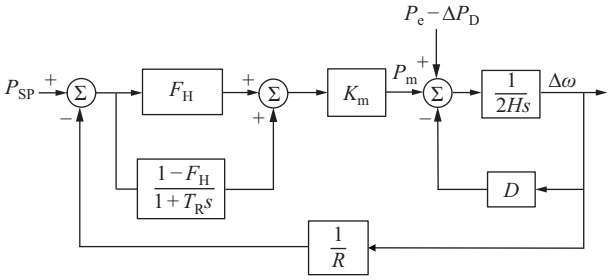

Fig. 2. The block diagram of the SFR model.

TABLE III
EQUIVALENT PARAMETERS OF ISOLATED POWER SYSTEM IN THE SFR MODEL

T_R	H	F_H	D	R	K_m
1.205	1.246	0.077	1.000	0.050	0.820

TABLE IV
OUTPUT POWER OF GENERATORS AND WIND FARMS

G1/G2	G3/G4	G5/G6	G7/G8	W1/W2
58.4 MW	87.2 MW	168.5 MW	195.4 MW	210.8 MW

due to short circuit fault, this can lead to a huge active power imbalance of 168.5 MW in the isolated power system. The rest of the thermal generators are able to provide primary frequency reserve as 75 MW (5% of the installed capacity). At $t = 2$ s, the line between G5 and the Bus 9 is broken, which causes G5 to trip off from the system. The initial variance ratio of the frequency, $\mathrm{d}f/\mathrm{d}t|_{t=2\,\mathrm{s}}$, is 4.426 Hz/s. The frequency response curve of the isolated power system is shown in Fig. 3(a). The system frequency drops down to a nadir of 48.5 Hz in seconds and finally keeps steady at 49.5 Hz.

Load shedding is not practical for electrolytic aluminum loads because it can only be shed as a whole part. The power demand of three aluminum loads are 330 MW, 420 MW and 640 MW, respectively. The frequency response curve after shedding aluminum load 1 at $t = 2.5$ s is shown in Fig. 3(b). The peak of the frequency is 50.75 Hz when the aluminum load 1 is shed at 0.5 s after the emergency occurs, which may result in activation of the generator over-frequency protection

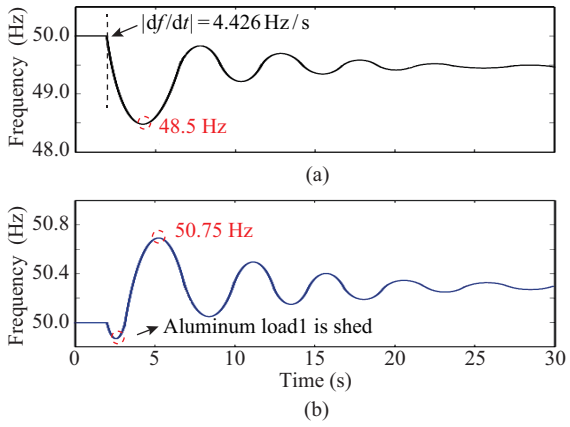

Fig. 3. Isolated power system frequency results. (a) Isolated power system frequency when G5 is out of service. (b) Isolated power system frequency after aluminum load1 is shed.

and system collapses. Obviously, it is difficult to maintain the stability in a transient state. The reasons are summarized as follows:

1) The capacity of a single generator or load is too large compared to the total installed capacity. The wind power penetration is 30.8% of total generation capacity. The primary frequency reserve power from generators is not enough for the large power imbalance. The fault of one load or generator will dramatically impact the power balance in the isolated power system.

2) The inertia of the system is very small due to the disconnection with the utility power grid, leading to frequency collapse in a very short time.

In order to keep stable and safe operations for the isolated power system with such extreme scenarios, the following emergency control schemes may need to be applied:

1) Construct a tie-line between the isolated power system and utility power grid. As a result, active power imbalance can be compensated by public power companies to maintain the frequency stability. However, the huge electricity cost ($9.14 million per year) and additional charges for the construction and maintenance have to be paid by industrial consumer [26]. Therefore, such a scheme is not financially sound nor practically feasible.

2) Decrease the active power consumption of aluminum loads. The reason why the load shedding is not practical for aluminum loads has been analyzed above. Since an electrolytic aluminum load can be modeled as a voltage-dependent load, the papers [9], [10] have studied voltage regulation on the demand side, to reduce the power demand of the electrolytic aluminum load. In this way, the power imbalance in the isolated power system can be compensated. Although the voltage regulation is an effective method, the quality of production is, to a certain extent, compromised.

In view of the drawbacks of the control methods discussed above and high wind power penetration (30.8% of total generation capacity with strong nonlinearity) in the isolated power system, we propose in this paper a frequency control scheme from a generation side and nonlinear perspective. Previous studies have demonstrated the possibility and potential of frequency regulation by using variable speed wind turbines (e.g., DFIGs) [30]–[33]. By comparison, this study concentrates on the development of a coordinated frequency control approach that combines thermal generators with DFIGs in extreme scenarios, e.g., one with generators being out of service. We focus on the issue of how to compensate the active power imbalance more effectively in the presence of strong nonlinearity caused by wind power. In particular, a nonlinear coordinated frequency control scheme is developed, based on the nonlinear regulator theory, which is to be introduced and reviewed in Section IV.

III. ISOLATED POWER SYSTEM MODELLING

To develop an effective nonlinear coordinated frequency control scheme, we build in this section a dynamic model for the isolated power system with high penetration of wind power (DFIGs). In particular, an aerodynamic model and

the operational characteristics of wind turbines are presented. Then, a load frequency control model is derived to integrate the generators and DFIGs in the isolated power system, which serves as a foundation for the development of frequency regulation nonlinear control strategies presented in Section IV.

A. Rotor Speed Control (RSC) and Pitch Angle Control (PAC)

Generally, a wind farm can be represented by an aggregated model of a DFIG wind turbine, which has been a typical modelling method for power systems with high penetration of wind power [34]. The structure of a grid-connected DFIG wind turbine and control system is shown in Fig. 4.

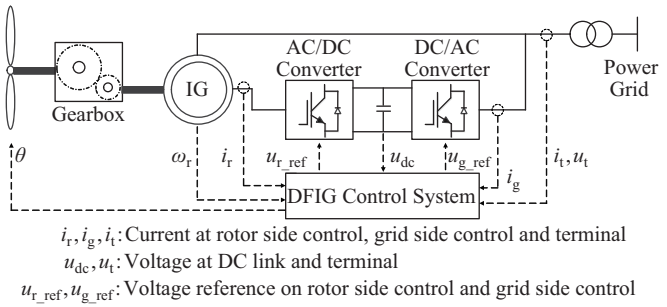

Fig. 4. A typical configuration of a DFIG.

It is known that the mechanical output power of wind turbine $P_{\rm wm}$ is expressed by (see, for instance, [35])

$$P_{\rm wm} = \frac{1}{2} C_{\rm p}(\lambda, \theta) \rho A V_{\rm w}^3 \tag{1}$$

$$C_{\rm p}(\lambda, \theta) = c_1 \left(\frac{c_2}{\lambda_i} - c_3\theta - c_4\theta^{c_5} - c_6 \right) e^{-c_7/\lambda_i} \tag{2}$$

$$\lambda = \omega_{\rm r} R / V_{\rm w} \tag{3}$$

$$\lambda_i = \left(\frac{1}{\lambda + 0.08\theta} - \frac{0.035}{\theta^3 + 1} \right)^{-1} \tag{4}$$

where ρ is the air density, A is the blade swept area, $V_{\rm w}$ is the wind speed, and $C_{\rm p}(\lambda, \theta)$ is the power coefficient defined by (2), with the parameters $c_1 = 0.5$, $c_2 = 116$, $c_3 = 0.4$, $c_4 = 0$, $c_5 = 2$, $c_6 = 5$, $c_7 = 21$ [35]. The coefficients λ and θ in (2) are the tip speed ratio and pitch angle, respectively. λ is expressed by (3), where $\omega_{\rm r}$ and R are turbine rotor speed and blade radius.

Figure 5(a) shows the curves of $P_{\rm wm}$ with $\omega_{\rm r}$ at various pitch angles (θ_1, θ_2 and θ_3). The green curve indicates that a wind turbine is operated under maximum power point tracking (MPPT) mode, and thus there is no participation from the wind turbine for frequency regulation. However, compared with a wide-area grid, an isolated power system, especially with high percentage renewable energy, is more vulnerable to power disturbance. In such a case, it is required that the wind turbine works under deloaded operation to provide a power reserve for frequency regulation [30]. The wind turbine may be deloaded by working at the left side (point C) or right side (point B) of the maximum power point A. The left operation point is unstable and likely to cause the turbine to stall when the grid frequency drops [36]. Thus, it is supposed that the wind turbine operates at the right side to provide power reserves. In this

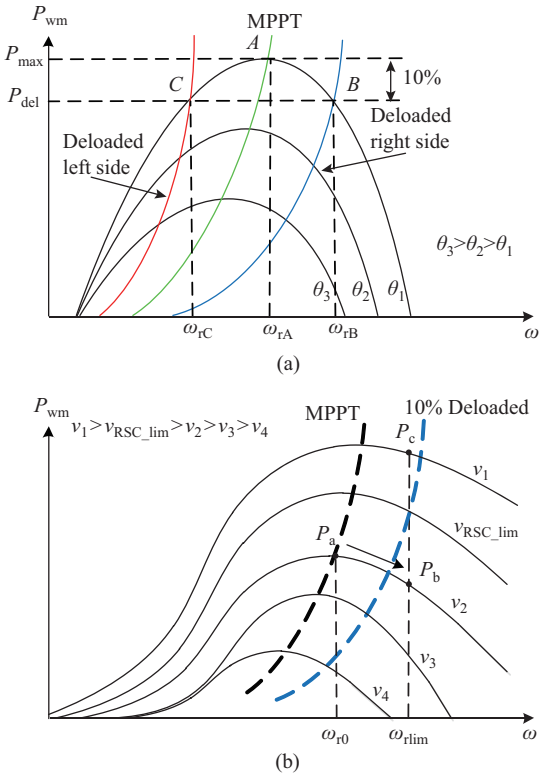

Fig. 5. The mechanical output power of wind turbine. (a) MPPT and deloaded power curves of wind turbine at certain wind speed. (b) 10% deloaded operation power curve with a rotor speed constraint.

paper, a deloaded margin of 10% is considered for DFIG, as demonstrated in Fig. 5(a).

Normally, the rotor speed reaches its maximum $\omega_{\rm lim}$ (usually 1.2 p.u.) at the rated wind speed $V_{\rm rate}$, i.e., the power of the wind turbine is able to be at rated capacity. As discussed above, a deloaded margin of DFIGs (generally set as 10%) is essential to the fast frequency regulation from DFIGs in the isolated power system.

RSC is aimed to track the power command through regulating rotor speed while the pitch angle is fixed. The rotor needs to absorb extra energy to increase its speed, which may result in a drop of the output power. In this case, the rotor speed varies in certain ranges when RSC is activated. Specifically, let us take the power curve at v_2 as an example shown in Fig. 5(b). When the rotor speed accelerates from $\omega_{\rm r0}$ to its upper limit $\omega_{\rm rlim}$, output power decreases from P_a to P_b. Assuming that under certain wind speed $V_{\rm RSC\text{-}lim}$ (wind speed limit for RSC), the wind turbine is permitted to work at 10% deloaded margin operation at $\omega_{\rm rlim}$ by only applying to RSC. When the wind speed is higher than $V_{\rm RSC\text{-}lim}$, the output power regulated by RSC would reach its limit with the rotor speed reaching $\omega_{\rm rlim}$. For instance, for the power curve at V_1 in Fig. 5(b), the output power cannot be tracked to the value lower than $P_{\rm c}$ using only RSC.

To overcome the limitation of RSC, PAC has been considered as an alternative strategy to further regulate the output power by adjusting the pitch angle. Fig. 5(a) implies that the output power is lower when the pitch angle increases. Therefore, when the wind speed is higher than $V_{\rm RSC\text{-}lim}$, PAC

is able to effectively regulate the output power to satisfy the requirements of a deloaded operation when $\omega_{\rm rlim}$ reaches its upper limit. The characteristics of the aforementioned two control methods are quite different. In terms of response, RSC is better because the output power decreases smoothly with less time in a narrow range. By comparison, PAC provides a wider regulating range of the output power and a slower response due to the characteristics of pitch angle systems.

In view of discussions so far, we propose in this study to combine RSC with PAC under various wind speed $V_{\rm w}$, based on the following principles.

1) Low wind speed ($V_{\rm w} < V_{\rm RSC\text{-}lim}$):

Implementing RSC is sufficient to the requirement of 10% deloaded margin operation.

2) Medium wind speed ($V_{\rm RSC\text{-}lim} \le V_{\rm w} < V_{\rm rate}$):

RSC is activated to maintain the rotor speed in upper limit $\omega_{\rm lim}$ (1.2 p.u.), while PAC is applied to further regulate the output power for guaranteeing 10% deloaded operation.

3) High wind speed ($V_{\rm w} \ge V_{\rm rate}$):

In this case, the rotor speed reaches $\omega_{\rm lim}$. Thus, PAC is applied to keep wind turbine operating at deloaded mode.

Using the principles listed above, we shall develop a coordinated frequency control model of generators and DFIGs under various wind speeds in the next subsection.

B. Load Frequency Control (LFC) Model of Isolated Power System

Considering an isolated power system that contains m generators and n DFIG-based wind turbines as shown in Fig. 6, a block diagram of the LFC model is given.

In Fig. 6, M and D are the equivalent inertia constant and load damping constant of the power system, respectively. Δf is the frequency deviation in the power system. The power disturbance is represented by ΔP_D. Areas 1 and 2 represent the control model of conventional generators and DFIG-based wind turbines, respectively. For the i-th generator, R_i, $P_{{\rm gref}i}$ and $\Delta X_{\rm Gi}$ are the droop control coefficient, control input and valve position deviation. $T_{\rm RHi}$ and $\Delta P_{\rm RHi}$ are the time constant and the output power deviation of reheater. $K_{\rm HPi}$ is the fraction of turbine power generated by the high pressure unit. $\Delta P_{\rm Gi}$ is the output power deviation of the steam turbine, with the maximal value $\Delta P_{\rm Gimax}$ and the minimal value $\Delta P_{\rm Gimin}$. $T_{\rm Gi}$ and $T_{\rm Ti}$ are the time constants of the speed governor and steam turbine. For the j-th DFIG,

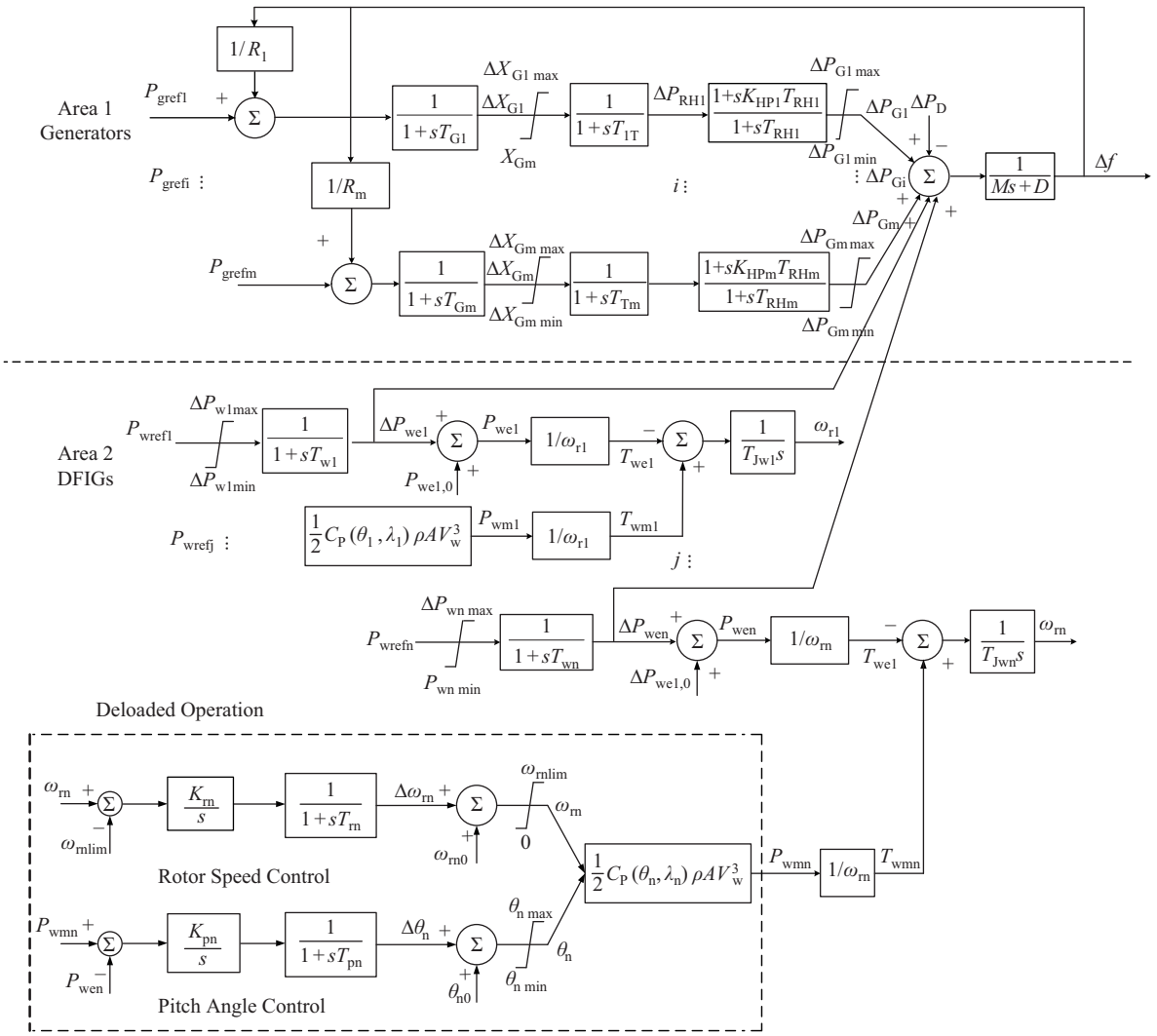

Fig. 6. LFC model of isolated power system.

the control input is $P_{\mathrm{wref}j}$, with the maximal and minimal values expressed as $\Delta P_{\mathrm{wjmax}}$ and $\Delta P_{\mathrm{wjmin}}$. $\Delta P_{\mathrm{we}j}$ is the electromagnetic power deviation of DFIG.

As discussed in subsection A, when the wind speed V_{w} is lower than $V_{\mathrm{RSC\text{-}lim}}$, RSC is adopted to realize deloaded operation of the wind turbine, while PAC is employed when V_{w} is higher than $V_{\mathrm{RSC\text{-}lim}}$. The state space models under various wind speeds are developed as follows.

Case 1: $V_{\mathrm{w}} \le V_{\mathrm{RSC\text{-}lim}}$

In this case, only RSC is implemented to adjust the output power of DFIGs. According to Fig. 6, the rotor equation of DFIGs is described as:

$$\omega_{\mathrm{r}j}\dot{\omega}_{\mathrm{r}j} = -\frac{1}{T_{\mathrm{Jw}j}}\left(\Delta P_{\mathrm{we}j} + P_{\mathrm{we}j,0}\right) + \frac{1}{T_{\mathrm{Jw}j}} P_{\mathrm{wm}j}\left(\omega_{\mathrm{r}j}, \theta_j\right) \tag{5}$$

where $P_{\mathrm{wm}j}(\omega_{\mathrm{r}j}, \theta_j)$ is the mechanical output power of the j-th DFIG, given by the nonlinear equations (1)–(4).

Define $\Delta\omega_{\mathrm{r}j}$ as

$$\Delta\omega_{\mathrm{r}j} = \omega_{\mathrm{r}j}^2 - \omega_{\mathrm{r}j,0}^2 \tag{6}$$

Thus, its derivative is given by:

$$\Delta\dot{\omega}_{\mathrm{r}j} = -\frac{2}{T_{\mathrm{Jw}j}}\Delta P_{\mathrm{we}j} + \frac{2}{T_{\mathrm{Jw}j}}\left[P_{\mathrm{wm}j}(\Delta\omega_{\mathrm{r}j}, \Delta\theta_j) - P_{\mathrm{we}j,0}\right] \tag{7}$$

Since no PAC is involved in a low wind speed scenario, $\Delta\theta_j = 0$. As a result, the state space model of the isolated power system is described by:

$$\begin{cases} \Delta\dot{f} = -\frac{D}{M}\Delta f + \frac{1}{M}\Delta P_{\mathrm{G}i} + \frac{1}{M}\Delta P_{\mathrm{we}j} - \frac{1}{M}\Delta P_D \\ \Delta\dot{P}_{\mathrm{G}i} = -\frac{1}{T_{\mathrm{RH}i}}\Delta P_{\mathrm{G}i} + \left(\frac{1}{T_{\mathrm{RH}i}} - \frac{F_{\mathrm{HP}i}}{T_{\mathrm{T}i}}\right)\Delta P_{\mathrm{RH}i} \\ \qquad + \frac{F_{\mathrm{HP}i}}{T_{\mathrm{T}i}}\Delta X_{\mathrm{G}i} \\ \Delta\dot{P}_{\mathrm{RH}i} = -\frac{1}{T_{\mathrm{T}i}}\Delta P_{\mathrm{RH}i} + \frac{1}{T_{\mathrm{T}i}}\Delta X_{\mathrm{G}i} \\ \Delta\dot{X}_{\mathrm{G}i} = -\frac{1}{T_{\mathrm{G}i}R_i}\Delta f - \frac{1}{T_{\mathrm{G}i}}\Delta X_{\mathrm{G}i} + \frac{1}{T_{\mathrm{G}i}}P_{\mathrm{gref}i} \\ \Delta\dot{P}_{\mathrm{we}j} = -\frac{1}{T_{\mathrm{s}i}}\Delta P_{\mathrm{we}j} + \frac{1}{T_{\mathrm{s}i}}P_{\mathrm{wref}j} \\ \Delta\dot{\omega}_{\mathrm{r}j} = -\frac{2}{T_{\mathrm{Jw}j}}\Delta P_{\mathrm{we}j} \\ \qquad + \frac{2}{T_{\mathrm{Jw}j}}\left[P_{\mathrm{wm}j}(\Delta\omega_{\mathrm{r}j}, \Delta\theta_j) - P_{\mathrm{we}j,0}\right] \end{cases} \tag{8}$$

Case 2: $V_{\mathrm{w}} > V_{\mathrm{RSC\text{-}lim}}$

When V_{w} is higher than $V_{\mathrm{RSC\text{-}lim}}$, PAC is implemented to maintain the deloaded operation of DFIG. For this reason, the following equations need to be added into (8), i.e.,

$$\dot{\theta}_{\mathrm{p}j} = k_{\mathrm{p}j}(P_{\mathrm{wm}j}(\Delta\omega_{\mathrm{r}j}, \Delta\theta_j) - P_{\mathrm{we}j}) \tag{9}$$

$$\Delta\dot{\theta}_j = -\frac{1}{T_{\mathrm{p}j}}\Delta\theta_j + \frac{1}{T_{\mathrm{p}j}}\theta_{\mathrm{p}j} \tag{10}$$

Combining (5) and (6), (9) can be rewritten as:

$$\dot{\theta}_{\mathrm{p}j} = \frac{k_{\mathrm{p}j}T_{\mathrm{Jw}j}}{2}\Delta\dot{\omega}_{\mathrm{r}j} \tag{11}$$

Because the initial states $\Delta\omega_{\mathrm{r}j}(0) = 0$ and $\theta_{\mathrm{p}j}(0) = 0$, (11) is simplified as:

$$\theta_{\mathrm{p}j} = \frac{k_{\mathrm{p}j}T_{\mathrm{Jw}j}}{2}\Delta\omega_{\mathrm{r}j} \tag{12}$$

Consequently, (10) reduces to:

$$\Delta\dot{\theta}_j = -\frac{1}{T_{\mathrm{p}j}}\Delta\theta_j + \frac{k_{\mathrm{p}j}T_{\mathrm{Jw}j}}{2T_{\mathrm{p}j}}\Delta\omega_{\mathrm{r}j} \tag{13}$$

Therefore, the state space equations of the LFC model of the isolated power with medium and high wind speeds are described by (8) and (13).

In summary, (8) and (8)–(13) are the nonlinear coordinated frequency control models under different wind speeds, which have considered the strong nonlinearity caused by wind power generation (see (1)–(4)) in the isolated power system.

IV. Coordinated Frequency Control Scheme based on Nonlinear Regulator Theory

To design the coordinated frequency control scheme, we take frequency deviation Δf as the output value of the control system. The power disturbance ΔP_D is considered as an external disturbance signal. The aim of the coordinated frequency control scheme is to increase fast frequency regulation ability and restore the frequency to the normal value (i.e., $\Delta f = 0$) when ΔP_D exists in the power system (8) (low wind speed) or (8)–(13) (medium or high wind speed). Due to the high penetration of DFIG-based wind power, the LFC model (8) or (8)–(13) presents a strong nonlinearity. In the presence of the disturbance ΔP_D and strong nonlinearity in (8) or (8)–(13), the coordinated frequency control is formulated as a nonlinear regulator problem, as shown in subsection C. Consequently, we can solve the frequency regulation problem for the nonlinear system (8) or (8)–(13) based on the nonlinear regulator theory [37]. The solution for the nonlinear regulator problem is to design the feedback controller to achieve control goals. In terms of the coordinated frequency scheme in the isolated power system, we need to find a practically feasible frequency controller for coordinating thermal generators and DFIGs when large power imbalance exists. By using nonlinear regulator theory, a coordinated frequency control scheme with the feedback control signals including Δf and ΔP_D is developed, in which the details are shown in subsection C.

With this idea in mind, we first review in this section the nonlinear regulator theory and show how it can be applied to design coordinated frequency controllers for the power systems (8) and (8)–(13).

A. Nonlinear Regulator Theory

Consider a power system that is described by a set of nonlinear differential equations of the form:

$$\begin{cases} \dot{\boldsymbol{x}} = \boldsymbol{f}(\boldsymbol{x}) + \boldsymbol{g}(\boldsymbol{x})\boldsymbol{u} + \boldsymbol{p}(\boldsymbol{x})\boldsymbol{w} \\ \dot{\boldsymbol{w}} = \boldsymbol{S}(\boldsymbol{w}) \\ \boldsymbol{e} = \boldsymbol{h}(\boldsymbol{x}) + \boldsymbol{q}(\boldsymbol{w}) \end{cases} \tag{14}$$

where the first equation describes a controlled plant with the state $\boldsymbol{x} \in \boldsymbol{R}^{\mathrm{r}}$, control input $\boldsymbol{u} \in \boldsymbol{R}^{\mathrm{p}}$ and external signal $\boldsymbol{w} \in \boldsymbol{R}^{\mathrm{s}}$. The second equation represents the disturbance (resp. reference) signals to be rejected (resp. tracked), generated by an exosystem. The third equation defines the error signal $\boldsymbol{e} \in \boldsymbol{R}^{q}$ between the output $\boldsymbol{y} = \boldsymbol{h}(\boldsymbol{x})$ and the reference $\boldsymbol{y}_{\mathrm{r}} = -\boldsymbol{q}(\boldsymbol{w})$.

The control objective is to find, if possible, a full-information feedback controller of the form:

$$\boldsymbol{u} = \boldsymbol{\alpha}(\boldsymbol{x}, \boldsymbol{w}) \tag{15}$$

such that the following two requirements are satisfied:

i) local asymptotical stability. When $\boldsymbol{w} = \boldsymbol{0}$, the system $\dot{\boldsymbol{x}} = \boldsymbol{f}(\boldsymbol{x}) + \boldsymbol{g}(\boldsymbol{x})\boldsymbol{\alpha}(\boldsymbol{x}, \boldsymbol{0})$ is locally asymptotically stable at the equilibrium $\boldsymbol{x} = \boldsymbol{0}$;

ii) error regulation. When $\boldsymbol{w} \neq \boldsymbol{0}$, for all initial conditions $(\boldsymbol{x}_0, \boldsymbol{w}_0) \subset \boldsymbol{U}$ that is a neighborhood in $\boldsymbol{X} \times \boldsymbol{W}$ of $(x, w) = (0, 0)$, the closed-loop system (14)–(15) satisfies $\lim_{t\to\infty} \boldsymbol{e}(t) = \lim_{t\to\infty}(\boldsymbol{h}(x(t)) + \boldsymbol{q}(w(t))) = 0$.

To solve the nonlinear regulator problem, the following two assumptions are required.

A1) $\boldsymbol{w} = \boldsymbol{0}$ is the Poisson stable equilibrium of $\dot{\boldsymbol{w}} = \boldsymbol{S}(\boldsymbol{w})$.

A2) The linearized system $\dot{\boldsymbol{x}} = \boldsymbol{A}\boldsymbol{x} + \boldsymbol{B}\boldsymbol{u}$ is stabilizable, where $\boldsymbol{A} = [\partial \boldsymbol{f}/\partial \boldsymbol{x}]_{\boldsymbol{x}=\boldsymbol{0}}$ and $\boldsymbol{B} = \boldsymbol{g}(\boldsymbol{0})$.

With the help of the assumptions above, a necessary and sufficient condition can be derived for the solvability of the nonlinear regulator problem [37].

Proposition 4.1: Under A1) and A2), the output regulation problem is solvable by full-information feedback if and only if there exists $C^k(k > 1)$ mappings $\boldsymbol{x} = \boldsymbol{\pi}(\boldsymbol{w})$, with $\boldsymbol{\pi}(\boldsymbol{0}) = \boldsymbol{0}$, and $\boldsymbol{u} = \boldsymbol{c}(\boldsymbol{w})$, with $\boldsymbol{c}(\boldsymbol{0}) = \boldsymbol{0}$, both defined in a neighborhood $\boldsymbol{W}_0 \subset \boldsymbol{W}$ containing origin, satisfying the regulator equations

$$\frac{\partial \boldsymbol{\pi}}{\partial \boldsymbol{w}}\boldsymbol{S}(\boldsymbol{w}) = \boldsymbol{f}[\boldsymbol{\pi}(\boldsymbol{w})] + \boldsymbol{g}[\boldsymbol{\pi}(\boldsymbol{w})]\boldsymbol{c}(\boldsymbol{w}) + \boldsymbol{p}[\boldsymbol{\pi}(\boldsymbol{w})]\boldsymbol{w} \tag{16}$$

$$\boldsymbol{0} = \boldsymbol{h}[\boldsymbol{\pi}(\boldsymbol{w})] + \boldsymbol{q}(\boldsymbol{w}) \tag{17}$$

As a consequence, the following feedback controller

$$\boldsymbol{u} = \boldsymbol{\alpha}(\boldsymbol{x}, \boldsymbol{w}) = \boldsymbol{c}(\boldsymbol{w}) + \boldsymbol{K}[\boldsymbol{x} - \boldsymbol{\pi}(\boldsymbol{w})] \tag{18}$$

solves the nonlinear regulator problem, i.e., the goals i) and ii) are achieved.

The gain matrix $\boldsymbol{K}$ in (18) is selected based on the pole assignment, so that all the eigenvalues of $\boldsymbol{A}+\boldsymbol{B}\boldsymbol{K}$ are located on the open left-half plane. On the other hand, $\boldsymbol{\pi}(\boldsymbol{w})$ and $\boldsymbol{c}(\boldsymbol{w})$ are solved from the regulator equations (16)–(17).

B. Controller Design Procedure

The frequency controllers for the power system (8) or (8)–(13) can be designed via *Proposition 4.1*. For the convenience of the reader, we present in this subsection a design algorithm. In the next subsection, we shall apply the algorithm below to find the coordinated frequency controllers.

1) Check the assumption A1) for the power system (8) or (8)–(13). Because the disturbance ΔP_D is the imbalance of active power, and thus a constant. Then, $\boldsymbol{w} = \Delta P_D$ satisfies $\dot{\boldsymbol{w}} = \boldsymbol{S}(\boldsymbol{w}) = \boldsymbol{0}$, i.e., the exosystem is a Poisson stable. In other words, the assumption A1) holds in this paper.

2) To check the assumption A2), one needs to find the linearization pair $\boldsymbol{A} = [\partial \boldsymbol{f}/\partial \boldsymbol{x}]_{\boldsymbol{x}=\boldsymbol{0}}$ and $\boldsymbol{B} = \boldsymbol{g}(\boldsymbol{0})$ of the power system (8) or (8)–(13), and then use the PBH test below to compute the rank condition:

$$\mathrm{Rank}([\mu \boldsymbol{I} - \boldsymbol{A} \quad \boldsymbol{B}]) = n_{\mathrm{dim}} \tag{19}$$

where n_{dim} is the dimension of the power system (8) or (8)–(13) and μ is every eigenvalue of the matrix $\boldsymbol{A}$ sitting on the closed right-half plane.

3) If A1) and A2) hold, a pair of solutions $\pi(w)$ and $c(w)$ is obtained by solving the regulator equations (16)–(17). Notably, the partial differential equation (PDE) (16) can be dramatically simplified because $\boldsymbol{S}(\boldsymbol{w}) = \boldsymbol{0}$. As a result, the PDE (16) reduces to a nonlinear algebraic equation:

$$\boldsymbol{0} = \boldsymbol{f}[\boldsymbol{\pi}(\boldsymbol{w})] + \boldsymbol{g}[\boldsymbol{\pi}(\boldsymbol{w})]\boldsymbol{c}(\boldsymbol{w}) + \boldsymbol{p}[\boldsymbol{\pi}(\boldsymbol{w})]\boldsymbol{w} \tag{20}$$

Thus, solving $\boldsymbol{\pi}(\boldsymbol{w})$ and $\boldsymbol{c}(\boldsymbol{w})$ becomes a relatively easy task. See subsection C for details.

4) Find the gain matrix $\boldsymbol{K}$ by the pole assignment [38] such that all the eigenvalues of the matrix $\boldsymbol{A} + \boldsymbol{B}\boldsymbol{K}$ are located on the open left-half plane.

5) Use the functions $\boldsymbol{\pi}(\boldsymbol{w})$ and $\boldsymbol{c}(\boldsymbol{w})$ obtained from Step 3) and the gain matrix $\boldsymbol{K}$ from Step 4) to construct the feedback controller (18).

Although the feedback controller (18) solves the frequency regulation problem, it is impractical and not implementable because it requires that all the components of the state $\boldsymbol{x}$ in the power system (8) or (8)–(13) be measurable. To realize the proposed frequency control scheme, we need to refine the feedback controller (18) by using measurable signals only to obtain a practical feasible controller.

6) For the normal operation of the isolated power system (8) or (8)–(13), note that the nonlinear system (8) or (8)–(13) is locally stable without control. Indeed, all the eigenvalues of $\boldsymbol{A}$ are located on the open left-half plane. Thus, one can take advantage of this nice stability property of the system (8) or (8)–(13) by replacing $\boldsymbol{K}$ with a more specific gain matrix $\boldsymbol{K}_s$ (see subsection C for details) that meets simultaneously two requirements: a) $\boldsymbol{A}+\boldsymbol{B}\boldsymbol{K}$ is Hurwitz; b) only measurable components of the state $\boldsymbol{x}$ are used for feedback. In this paper, we construct a realizable feedback controller as:

$$\boldsymbol{u} = \boldsymbol{c}(\boldsymbol{w}) + \boldsymbol{K}[\boldsymbol{x} - \boldsymbol{\pi}(\boldsymbol{w})] = \boldsymbol{K}_s\boldsymbol{y} + \boldsymbol{\varphi}(\boldsymbol{w}) \tag{21}$$

The feedback signals in (21) include t he frequency deviations Δf and power disturbance ΔP_D, which are measurable. Due to the structure of the isolated power system shown in Fig. 1, active power imbalances can be measured directly. Compared with (18), the controller (21) is implementable and practically feasible. However, the controller (21) cannot place the poles of $\boldsymbol{A}+\boldsymbol{B}\boldsymbol{K}$ arbitrarily nor significantly improve the system stability margin. Nevertheless, it does guarantee all the eigenvalues of $\boldsymbol{A} + \boldsymbol{B}\boldsymbol{K}$ are on the open left-half plane, and thus still achieves frequency regulation with internal stability for the nonlinear power system (8) or (8)–(13) locally.

Figure 7 demonstrates the detailed block diagram of the control scheme design procedure.

C. Frequency Controllers in Various Wind Speeds

To design a feasible frequency controller (21) for the actual isolated power system in Fig. 1, we must solve the functions $\boldsymbol{\pi}(\boldsymbol{w})$ and $\boldsymbol{c}(\boldsymbol{w})$ from the nonlinear algebraic equations (20) and (17). In this subsection, we first design the coordinated frequency controller for a simple power system with only a single

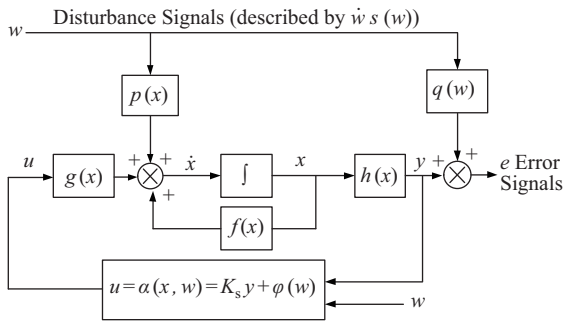

Fig. 7. The block diagram of the control scheme design procedure.

generator and single DFIG. Due to the simple configuration and one-way power flow characteristic of the isolated power system, the frequency controllers for multiple generators and DFIGs can then be deduced.

Case 1: $V_{\rm w} \le V_{\rm RSC\text{-}lim}$

This is the case when wind speed is low. In this case, the power system (8) is of the form (14), where the state $\boldsymbol{x} = [\Delta \boldsymbol{f}, \Delta \boldsymbol{P}_{\rm Gi}, \Delta \boldsymbol{P}_{\rm RHi}, \Delta \boldsymbol{X}_{\rm Gi}, \Delta \boldsymbol{P}_{{\rm we}j}, \Delta \boldsymbol{\omega}_{{\rm r}j}]^{\rm T} \in \boldsymbol{R}^{1+3m+2n}$, control input $\boldsymbol{u} = [\boldsymbol{P}_{{\rm gref}i}, \boldsymbol{P}_{{\rm wref}j}]^{\rm T} \in \boldsymbol{R}^{m+n}$, external signal $\boldsymbol{w} = \Delta \boldsymbol{P}_D \in \boldsymbol{R}$, output $\boldsymbol{y} = \Delta \boldsymbol{f} \in \boldsymbol{R}$ and the vector fields

$$\boldsymbol{f}(\boldsymbol{x}) = \begin{bmatrix} -\frac{D}{M}\Delta \boldsymbol{f} + \frac{1}{M}\Delta \boldsymbol{P}_{\rm Gi} + \frac{1}{M}\Delta \boldsymbol{P}_{{\rm we}j} \\ -\frac{1}{T_{{\rm RH}i}}\Delta \boldsymbol{P}_{\rm Gi} + \left(\frac{1}{T_{{\rm RH}i}} - \frac{F_{{\rm HP}i}}{T_{{\rm T}i}}\right)\Delta \boldsymbol{P}_{{\rm RH}i} + \frac{F_{{\rm HP}i}}{T_{{\rm T}i}}\Delta \boldsymbol{X}_{{\rm G}i} \\ -\frac{1}{T_{{\rm T}i}}\Delta \boldsymbol{P}_{{\rm RH}i} + \frac{1}{T_{{\rm T}i}}\Delta \boldsymbol{X}_{{\rm G}i} \\ -\frac{1}{T_{{\rm G}i}R_i}\Delta \boldsymbol{f} - \frac{1}{T_{{\rm G}i}}\Delta \boldsymbol{X}_{{\rm G}i} \\ -\frac{1}{T_{si}}\Delta \boldsymbol{P}_{{\rm we}j} \\ -\frac{2}{T_{{\rm J}wj}}\Delta \boldsymbol{P}_{{\rm we}j} + \frac{2}{T_{{\rm J}wj}}\left[P_{{\rm wm}j}\left(\Delta \boldsymbol{\omega}_{\boldsymbol{rj}}, \Delta \boldsymbol{\theta}_{\boldsymbol{j}}\right) - P_{{\rm we}j,0}\right] \end{bmatrix}$$

$$\boldsymbol{g}(\boldsymbol{x}) = \boldsymbol{B} = \begin{bmatrix} \boldsymbol{0} & \boldsymbol{0} \\ \boldsymbol{0} & \boldsymbol{0} \\ \boldsymbol{0} & \boldsymbol{0} \\ \boldsymbol{1/T}_{\rm Gi} & \boldsymbol{0} \\ \boldsymbol{0} & \boldsymbol{1/T}_{\rm si} \\ \boldsymbol{0} & \boldsymbol{0} \end{bmatrix} \in \boldsymbol{R}^{(1+3m+2n)\times(m+n)}$$

$$\boldsymbol{p}(\boldsymbol{x}) = \boldsymbol{E} = \left[-\frac{1}{\boldsymbol{M}}, \boldsymbol{0}, \boldsymbol{0}, \boldsymbol{0}, \boldsymbol{0}, \boldsymbol{0}\right]^{\rm T} \in \boldsymbol{R}^{(1+3m+2n)}$$

$$\boldsymbol{q}(\boldsymbol{w}) = 0$$

$$\boldsymbol{h}(\boldsymbol{x}) = \boldsymbol{C}\boldsymbol{x}, \boldsymbol{C} = [1, \boldsymbol{0}, \boldsymbol{0}, \boldsymbol{0}, \boldsymbol{0}, 0] \in \boldsymbol{R}^{1\times(1+3m+2n)}$$

For the simple power system with only a single generator and single DFIG, $m = n = 1$. Following the design procedure in subsection B, it is easy to verify that the power system (8) in low wind speed satisfies assumptions A1) and A2). Letting

$$\boldsymbol{x} = \boldsymbol{\pi} = [\pi_1(w), \pi_2(w), \pi_3(w), \pi_4(w), \pi_5(w), \pi_6(w)]^{\rm T}$$
$$\boldsymbol{u} = \boldsymbol{c}(\boldsymbol{w}) = [c_1(w), c_2(w)]^{\rm T}$$

and substituting them into eqn. (20) and (17), we obtain

$$\begin{cases} \pi_1(w) = 0 \\ \pi_2(w) = \pi_3(w) = \pi_4(w) \\ \pi_2(w) + \pi_5(w) - w = 0 \\ \pi_5(w) = P_{\rm wm}(\pi_6(w), 0) - P_{we.0} \end{cases}$$

$$\begin{cases} c_1(w) = \pi_2(w) \\ c_2(w) = \pi_5(w) \end{cases}$$

Because the solution is not unique, set $\pi_6(w) = k_{\rm pd}w$, where $k_{\rm pd}$ is a power distribution coefficient between generators and DFIGs. Then,

$$\begin{aligned} &\pi_1(w) = 0 \\ &\pi_2(w) = \pi_3(w) = \pi_4(w) = w - [P_{\rm wm}(k_{\rm pd}w, 0) - P_{{\rm we},0}] \\ &\pi_5(w) = P_{\rm wm}(k_{\rm pd}w, 0) - P_{{\rm we},0},\ \pi_6(w) = k_{\rm pd}w \\ &c_1(w) = \pi_2(w),\ c_2(w) = \pi_5(w) \end{aligned} \tag{22}$$

Next, we find the gain matrix $\boldsymbol{K}_s$ to construct the feedback controller (21). Using the special structure of the power system (8), $\boldsymbol{K}_s$ associated with only frequency deviations is denoted as $\boldsymbol{K}_s = (k_{{\rm g}i}, k_{{\rm w}j})^{\rm T}$, where $k_{{\rm g}i}$ and $k_{{\rm w}j}$ are the feedback gains of generators and DFIGs, respectively. Note that in frequency response, generators are usually involved with droop control. Thus, $k_{{\rm g}i}$ can be simply designed as 0, while $k_{{\rm w}j}$ can be obtained by a n Interval Linear Matrix Inequality (ILMI) method [39]. In the feedback controller (21), $\boldsymbol{K} = \boldsymbol{K}_s\boldsymbol{C}$ and $\boldsymbol{\varphi}(\boldsymbol{w}) = \boldsymbol{c}(\boldsymbol{w}) - \boldsymbol{K}_s\boldsymbol{C}\boldsymbol{\pi}(\boldsymbol{w})$.

Finally, we use the solutions (22) to get a frequency controller for the simple power system (8) in low wind speed as:

$$\begin{aligned} \boldsymbol{P}_{\rm ref} &= \begin{bmatrix} P_{\rm gref} \\ P_{\rm wref} \end{bmatrix} \\ &= \begin{bmatrix} 0 \\ k_{\rm w} \end{bmatrix}\Delta f + \begin{bmatrix} \Delta P_D - [P_{\rm wm}(k_{\rm pd}\Delta P_D, 0) - P_{{\rm we},0}] \\ P_{\rm wm}(k_{\rm pd}\Delta P_D, 0) - P_{{\rm we},0} \end{bmatrix} \end{aligned} \tag{23}$$

Similarly, by introducing the reserve power distribution coefficients for generators $k_{\rm gdi}$, the active power reserve provided by the generators can be allocated by the value of $k_{\rm gdi}$. Thus, by following the design procedure mentioned above, the frequency controller for the power system with multiple generators and DFIGs can be deduced as:

$$\begin{aligned} \boldsymbol{P}_{\rm ref} = \begin{bmatrix} P_{\rm gref1} \\ \vdots \\ P_{{\rm gref}m} \\ P_{\rm wref1} \\ \vdots \\ P_{{\rm wref}n} \end{bmatrix} = \begin{bmatrix} 0 \\ \vdots \\ 0 \\ k_{\rm w1} \\ \vdots \\ k_{{\rm w}n} \end{bmatrix}\Delta f + \\ \begin{bmatrix} k_{\rm gd1}\left[\Delta P_D - \sum_{j=1}^{n}\left[P(k_{{\rm pd}j}\Delta P_D, 0) - P_{{\rm we}j,0}\right]\right] \\ \vdots \\ k_{{\rm gd}m}\left[\Delta P_D - \sum_{j=1}^{n}\left[P(k_{{\rm pd}j}\Delta P_D, 0) - P_{{\rm we}j,0}\right]\right] \\ P_{\rm wm1}(k_{\rm pd1}\Delta P_D, 0) - P_{{\rm we1},0} \\ \vdots \\ P_{{\rm wm}n}(k_{{\rm pd}n}\Delta P_D, 0) - P_{{\rm we}n,0} \end{bmatrix} \end{aligned} \tag{24}$$

Case 2: $V_{\rm w} > V_{\rm RSC\text{-}lim}$

This is the case when wind speed is medium or high. The power system (8)–(13) is again described by (14), where the state $\tilde{\boldsymbol{x}} = [\boldsymbol{x}, \Delta \boldsymbol{\theta}_j]^{\rm T} \in \boldsymbol{R}^{1+3m+3n}$, control input $\tilde{\boldsymbol{u}} = \boldsymbol{u}$, external signal $\tilde{\boldsymbol{w}} = \boldsymbol{w}$, output $\tilde{\boldsymbol{y}} = \boldsymbol{y}$ and

$$\tilde{\boldsymbol{f}}(\tilde{\boldsymbol{x}}) = \begin{bmatrix} \boldsymbol{f}(\tilde{\boldsymbol{x}}) \\ -\frac{1}{T_{\rm pj}}\Delta \boldsymbol{\theta}_{\boldsymbol{j}} + \frac{k_{\rm pj}T_{{\rm J}wj}}{2T_{\rm pj}}\Delta \boldsymbol{\omega}_{\boldsymbol{rj}} \end{bmatrix}$$

$$\tilde{\boldsymbol{g}}(\tilde{\boldsymbol{x}}) = \tilde{\boldsymbol{B}} = \boldsymbol{B}$$
$$\tilde{\boldsymbol{p}}(\tilde{\boldsymbol{x}}) = \tilde{\boldsymbol{E}} = \left[-\frac{1}{\boldsymbol{M}}, \boldsymbol{0}, \boldsymbol{0}, \boldsymbol{0}, \boldsymbol{0}, \boldsymbol{0}, \boldsymbol{0}\right]^{\mathrm{T}} \in \boldsymbol{R}^{1+3m+3n}$$
$$\tilde{\boldsymbol{q}}(\tilde{\boldsymbol{w}}) = 0$$
$$\tilde{\boldsymbol{h}}(\tilde{\boldsymbol{x}}) = \tilde{\boldsymbol{C}}\tilde{x},\ \tilde{\boldsymbol{C}} = [1, \boldsymbol{0}, \boldsymbol{0}, \boldsymbol{0}, \boldsymbol{0}, \boldsymbol{0}, \boldsymbol{0}] \in \boldsymbol{R}^{1\times(1+3m+3n)}$$

The design procedure of the frequency controllers for the power system (8) and (13) in medium and high wind speeds can be repeated, in a manner similar to Case 1. However, there are some differences in Case 2.

In Case 2, the state $\tilde{\boldsymbol{x}}$ and $\tilde{\boldsymbol{u}}$ are given by:

$$\tilde{\boldsymbol{x}} = [\tilde{\pi}_1(\tilde{w}), \tilde{\pi}_2(\tilde{w}), \tilde{\pi}_3(\tilde{w}), \tilde{\pi}_4(\tilde{w}), \tilde{\pi}_5(\tilde{w}), \tilde{\pi}_6(\tilde{w}), \tilde{\pi}_7(\tilde{w})]^{\mathrm{T}}$$
$$\tilde{\boldsymbol{u}} = [\tilde{c}_1(\tilde{w}), \tilde{c}_2(\tilde{w})]^{\mathrm{T}}$$

Solving the regulator equations (20) and (17), we obtain:

$$\begin{aligned}
&\tilde{\pi}_1(\tilde{w}) = 0\\
&\tilde{\pi}_2(w) = \tilde{\pi}_3(w) = \tilde{\pi}_4(\tilde{w})\\
&\qquad = \tilde{w} - \left[\tilde{P}_{\mathrm{wm}}\left(\tilde{k}_{\mathrm{pd}}\tilde{w}, \tilde{k}_{\mathrm{pd}j}\frac{k_{\mathrm{p}}T_{\mathrm{Jw}}}{2}\tilde{w}\right) - \tilde{P}_{\mathrm{we},0}\right]\\
&\tilde{\pi}_5(\tilde{w}) = \tilde{P}_{\mathrm{wm}}\left(\tilde{k}_{\mathrm{pd}}\tilde{w}, \tilde{k}_{\mathrm{pd}j}\frac{k_{\mathrm{p}}T_{\mathrm{Jw}}}{2}\tilde{w}\right) - \tilde{P}_{\mathrm{we},0}\\
&\tilde{\pi}_6(\tilde{w}) = \tilde{k}_{\mathrm{pd}}\tilde{w},\ \tilde{\pi}_7(\tilde{w}) = \tilde{k}_{\mathrm{pd}}\frac{k_{\mathrm{p}}T_{\mathrm{Jw}}}{2}\tilde{w}\\
&\tilde{c}_1(\tilde{w}) = \tilde{\pi}_2(\tilde{w}),\ \tilde{c}_2(\tilde{w}) = \tilde{\pi}_5(\tilde{w})
\end{aligned} \tag{25}$$

Consequently, for the medium and high wind speeds, the frequency controllers for the power system (8) and (13) with single or multiple generators and DFIGs are designed, respectively, as:

$$\tilde{\boldsymbol{P}}_{\mathrm{ref}} = \begin{bmatrix}\tilde{P}_{\mathrm{gref}}\\ \tilde{P}_{\mathrm{wref}}\end{bmatrix} = \begin{bmatrix}0\\ \tilde{k}_{\mathrm{w}}\end{bmatrix}\Delta f + \begin{bmatrix}\Delta\tilde{P}_D - \left[\tilde{P}_{\mathrm{wm}}\left(\tilde{k}_{\mathrm{pd}}\Delta\tilde{P}_D, \tilde{k}_{\mathrm{pd}}\frac{k_{\mathrm{p}}T_{\mathrm{Jw}}}{2}\Delta\tilde{P}_D\right) - \tilde{P}_{\mathrm{we},0}\right]\\ \tilde{P}_{\mathrm{wm}}\left(\tilde{k}_{\mathrm{pd}}\Delta\tilde{P}_D, \tilde{k}_{\mathrm{pd}}\frac{k_{\mathrm{p}}T_{\mathrm{Jw}}}{2}\Delta\tilde{P}_D\right) - \tilde{P}_{\mathrm{we},0}\end{bmatrix} \tag{26}$$

$$\tilde{\boldsymbol{P}}_{\mathrm{ref}} = \begin{bmatrix}\tilde{P}_{\mathrm{gref}1}\\ \vdots\\ \tilde{P}_{\mathrm{gref}m}\\ \tilde{P}_{\mathrm{wref}1}\\ \vdots\\ \tilde{P}_{\mathrm{wref}n}\end{bmatrix} = \begin{bmatrix}0\\ \vdots\\ 0\\ \tilde{k}_{w1}\\ \vdots\\ \tilde{k}_{wn}\end{bmatrix}\Delta f + \begin{bmatrix}\tilde{k}_{\mathrm{gd}1}\left[\Delta\tilde{P}_D - \sum_{j=1}^{n}\left[\tilde{P}\left(\tilde{k}_{\mathrm{pd}j}\Delta\tilde{P}_D, \tilde{k}_{\mathrm{pd}j}\frac{k_{\mathrm{p}j}T_{\mathrm{Jw}j}}{2}\Delta\tilde{P}_D\right) - \tilde{P}_{\mathrm{we}j,0}\right]\right]\\ \vdots\\ \tilde{k}_{\mathrm{gdm}}\left[\Delta\tilde{P}_D - \sum_{j=1}^{n}\left[\tilde{P}\left(\tilde{k}_{\mathrm{pd}j}\Delta\tilde{P}_D, \tilde{k}_{\mathrm{pd}j}\frac{k_{\mathrm{p}j}T_{\mathrm{Jw}j}}{2}\Delta\tilde{P}_D\right) - \tilde{P}_{\mathrm{we}j,0}\right]\right]\\ \tilde{P}_{\mathrm{wm}1}\left(\tilde{k}_{\mathrm{pd}1}\Delta\tilde{P}_D, \tilde{k}_{\mathrm{pd}1}\frac{k_{\mathrm{p}1}T_{\mathrm{Jw}1}}{2}\Delta\tilde{P}_D\right) - \tilde{P}_{\mathrm{we}1,0}\\ \vdots\\ \tilde{P}_{\mathrm{wm}n}\left(\tilde{k}_{\mathrm{pd}n}\Delta\tilde{P}_D, \tilde{k}_{\mathrm{pd}n}\frac{k_{\mathrm{p}n}T_{\mathrm{Jw}n}}{2}\Delta\tilde{P}_D\right) - \tilde{P}_{\mathrm{we}n,0}\end{bmatrix} \tag{27}$$

By selecting $k_{\mathrm{w}j}$ and $\tilde{k}_{\mathrm{w}j}$ in (24) and (27) appropriately, we can make DFIGs participate in the primary frequency control in a similar fashion as generators. The distribution of the reserve power between generators and DFIGs in the case of low (resp. medium and high) wind speed can be done by choosing the value of $k_{\mathrm{pd}j}$ (resp. $\tilde{k}_{\mathrm{pd}j}$).

V. Simulation and Analysis

To verify the performance of the proposed nonlinear frequency regulation controllers (24) and (27) for the isolated power system in Fig. 1, simulations are conducted in a real-time digital simulation (RTDS) platform. The capacity of the thermal generators and the loads are presented in Fig. 1. The two 400 MW DFIG-based wind farms are represented by two aggregated DFIG models with identical parameters. The rated wind speed V_{rate} is 10.9 m/s. The RSC wind speed limit $V_{\mathrm{RSC\text{-}lim}}$ for the DFIG model in this study is 9.3 m/s. The rated rotor speed of DFIG is 1500 r/min (1.1 p.u.). The base capacity in the power system S_{B} is 100 MVA. In simulations, two DFIGs operate with 10% deloaded mode.

In this section, we consider three cases to validate the effectiveness of the proposed coordinated frequency controllers in various wind speeds. In addition, we validate the robustness of the coordinated frequency controllers against the short term (at the seconds-level) wind speed fluctuations. To prove the better performance of the proposed coordinated frequency controllers, the PI controllers are simulated as the comparison. The parameters of the PI controllers are shown in the Appendix, in which the setting method has been introduced in detail in [40], [41].

Three cases (low wind speed, medium wind speed and high wind speed) are considered. For each case, simulations are conducted to illustrate the effectiveness of the frequency controller (24) and (27) when short term (at the seconds-level) wind speed fluctuations exist.

Case 1: Low wind speed ($V_{\mathrm{w}} < V_{\mathrm{RSC\text{-}lim}}$)

In this case, the initial wind speed for W1 and W2 are 8.5 m/s and 7.9 m/s, lower than $V_{\mathrm{RSC\text{-}lim}}$. The output power of generators and DFIGs is given in Table V.

TABLE V
Output Power of Generators and DFIGs in Case 1

G1/G2	G3/G4	G5/G6	G7/G8	W1	W2
56.5 MW	84.4 MW	168.7 MW	192.2 MW	230.8 MW	215.5 MW

The output powers of W1 and W2 that operate in 10% deloaded mode are 230.8 MW and 215.5 MW, respectively. Thus, the maximal value of reserve power from W1 and W2 are 25.6 MW and 23.9 MW respectively, which means $\Delta P_{\mathrm{w1max}} = 0.256$ p.u. and $\Delta P_{\mathrm{w2max}} = 0.239$ p.u.. At $t = 2$ s, the generator G7 is out of service due to a short circuit fault, resulting in a significant power imbalance $\Delta P_D = 1.922$ p.u. in the isolated power system. The wind speeds of W1 and W2 fluctuate within $\pm 10\%$ after the emergency, shown in Fig. 8.

We consider three scenarios to address the power imbalance problem, as shown in Table VI. In Scenario 1, the PI control scheme is designed by using the information of Δf for generators and DFIGs. In Scenarios 2 and 3, the power reserve from

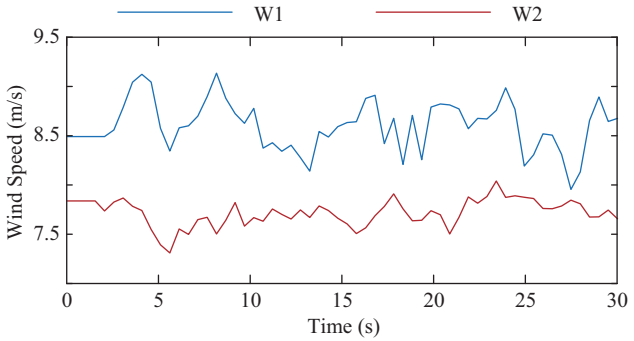

Fig. 8. The wind speeds fluctuations in Case 1.

TABLE VI
THE THREE OPERATING SCENARIOS IN CASE 1

Scenario 1	PI control scheme for generators and DFIGs
Scenario 2	coordinated frequency control scheme (24) set $P_{\mathrm{wm}j}(k_{\mathrm{pd}j}\Delta P_D) - P_{\mathrm{we}j,0} = 0 (j = 1, 2)$
Scenario 3	coordinated frequency control scheme (24) set $P_{\mathrm{wm}j}(k_{\mathrm{pd}j}\Delta P_D) - P_{\mathrm{we}j,0} = \Delta P_{\mathrm{wjmax}} (j = 1, 2)$

generators is distributed in proportion to installed capacity by selecting the corresponding coefficients k_{gdi}. We design nonlinear frequency regulation controllers in Scenarios 2 and 3. The objectives for two scenarios are to develop the frequency response ability from DFIGs and coordinate the power reserve among the generators and DFIGs. The differences are that we set $P_{\mathrm{wm}j}(k_{\mathrm{pd}j}\Delta P_D) - P_{\mathrm{we}j,0} = 0$ $(j = 1, 2)$ in Scenario 2 and $P_{\mathrm{wm}j}(k_{\mathrm{pd}j}\Delta P_D) - P_{\mathrm{we}j,0} = \Delta P_{\mathrm{wjmax}}$ $(j = 1, 2)$ in Scenario 3, with the controllers being presented in Table VII. The coordinated frequency control scheme in Scenario 2 indicates that the DFIGs provide frequency response (similar to the thermal generators) but no active power reserve. In Scenario 3, the frequency response and active power reserve from DFIGs are considered simultaneously.

TABLE VII
THE COORDINATED FREQUENCY CONTROLLERS FOR SCENARIO2 AND SCENARIO 3 IN CASE 1

Scenario 2

$$\boldsymbol{P}_{\mathrm{ref}} = \begin{bmatrix} P_{\mathrm{gref1}} \\ P_{\mathrm{gref2}} \\ P_{\mathrm{gref3}} \\ P_{\mathrm{gref4}} \\ P_{\mathrm{gref5}} \\ P_{\mathrm{gref6}} \\ P_{\mathrm{gref8}} \\ P_{\mathrm{wref1}} \\ P_{\mathrm{wref2}} \end{bmatrix} = \begin{bmatrix} 0 \\ 0 \\ 0 \\ 0 \\ 0 \\ 0 \\ 0 \\ -6.43 \\ -6.36 \end{bmatrix} \Delta f + \begin{bmatrix} 0.133 \\ 0.133 \\ 0.199 \\ 0.199 \\ 0.397 \\ 0.397 \\ 0.464 \\ 0 \\ 0 \end{bmatrix}$$

Scenario 3

$$\boldsymbol{P}_{\mathrm{ref}} = \begin{bmatrix} P_{\mathrm{gref1}} \\ P_{\mathrm{gref2}} \\ P_{\mathrm{gref3}} \\ P_{\mathrm{gref4}} \\ P_{\mathrm{gref5}} \\ P_{\mathrm{gref6}} \\ P_{\mathrm{gref8}} \\ P_{\mathrm{wref1}} \\ P_{\mathrm{wref2}} \end{bmatrix} = \begin{bmatrix} 0 \\ 0 \\ 0 \\ 0 \\ 0 \\ 0 \\ 0 \\ -6.43 \\ -6.36 \end{bmatrix} \Delta f + \begin{bmatrix} 0.098 \\ 0.098 \\ 0.148 \\ 0.148 \\ 0.295 \\ 0.295 \\ 0.345 \\ 0.256 \\ 0.239 \end{bmatrix}$$

Using the ILMI method, we calculate the feedback control coefficients k_{w1}, k_{w2} in Scenario 2, which are equal to -6.43 and -6.36 for W1 and W2, same as in Scenario 3. Consequently, the coordinated frequency controllers in Scenarios 2 and 3 can be obtained, respectively, as shown in Table VII.

At $t = 2$ s, there is a sudden loss of active power from the generators due to a short circuit fault on G7. In Scenario 1, the system frequency decreases to 48.1 Hz at $t = 4$ s, as shown in Fig. 8(a). Lacking the coordination between PI controllers, the frequency may not recover to normal ranges in a short

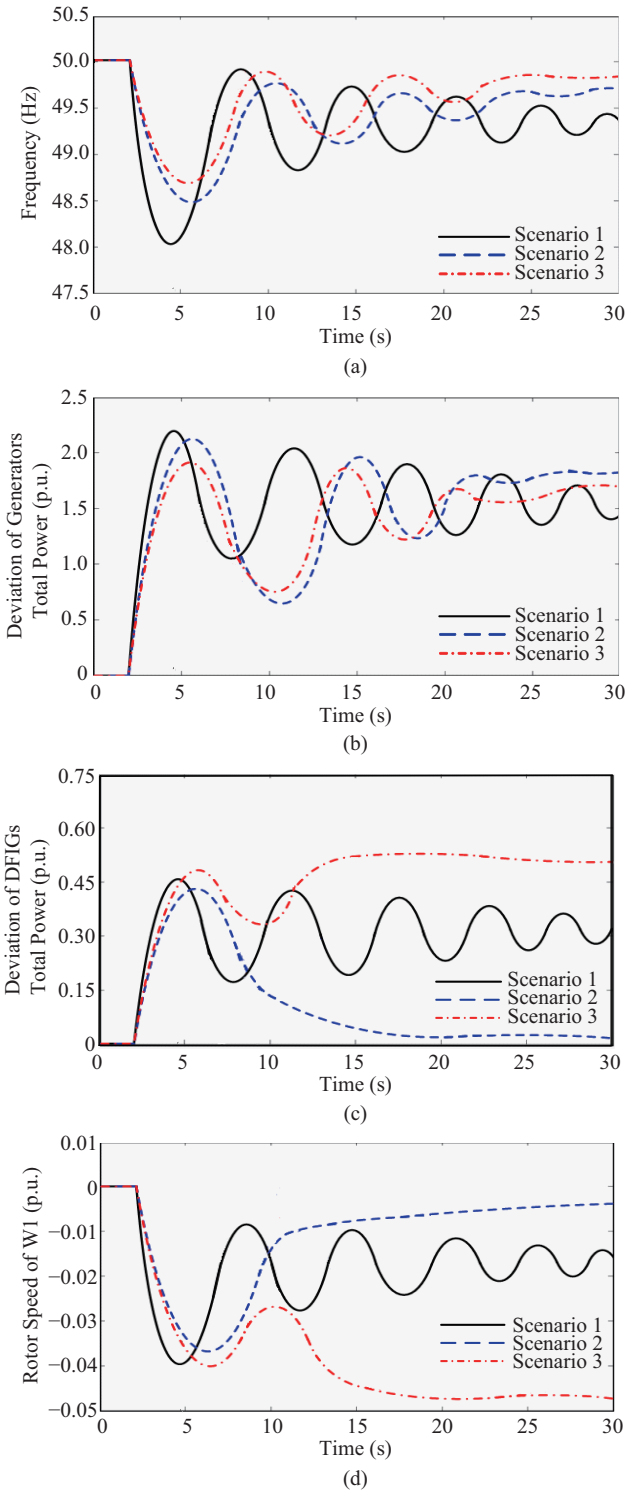

Fig. 9. Simulation results of three scenarios in Case 1. (a) Isolated power system frequency. (b) Total active power deviation of generators. (c) Total active power deviation of DFIGs. (d) Rotor speed of W1.

period of time. When the coordinated frequency controllers are applied in Scenario 2 and Scenario 3, the rate-of-change (ROC) and the nadir of frequency are improved when DFIGs participate in frequency regulation. The frequency recovers to normal range in seconds with an improved dynamic response, especially in Scenario 3. Fig. 9(b) and Fig. 9(c) present the total active power deviation of generators and DFIGs, respectively. Compared with Scenario 1, the generators and DFIGs in Scenario 2 and Scenario 3 are able to provide active power in a more stable way. In Scenario 2, the output power of DFIGs increases in a transient process (increases about 0.43 p.u.) and evenually restores to the initial value. Accordingly, the rotor speed of DFIGs in Scenario 2 decreases rapidly to release stored kinetic energy, and eventually recovers to the initial value, as shown in Fig. 9(d). In Scenario 3, DFIGs share the burden of providing reserve power of 0.495 p.u., with the rotor speed deviation decreasing about 0.05 p.u.. With the help of the DFIGs, the frequency has shown a better performance in the fast recovery process in Scenario 3 than in Scenario 2.

Case 2: High wind speed ($V_{\rm w} > V_{\rm RSC\text{-}lim}$)

In this case, we verify the effectiveness of the coordinated frequency controller (27) in high wind speed scenarios with fluctuations. The initial wind speeds $V_{\rm w}$ of W1 and W2 are 15 m/s and 14.3 m/s respectively and the output power of generators and DFIGs are given in Table VIII.

The proposed coordinated frequency controller (27) is validated by comparing with the PI controller, listed in Table IX.

The wind speed fluctuations are shown in Fig. 10. The emergency is that the generator G7 is out of service at $t =$ 2 s, resulting in the active power imbalance ΔP_D =1.419 p.u.. Using the ILMI method, we can obtain the feedback controller gains that $k_{\rm w1} = k_{\rm w2} = -6.72$. The results in Case 1 have indicated that the power system has a better performance in terms of frequency regulation when DFIGs provide reserve power. In order to get a fast frequency recovery, we select appropriate values of $\tilde{k}_{{\rm pd}j}$ in Case 2 such that each DFIG provides reserve power to its maximum. The reserve power from generators is distributed in proportion to installed capacity. The coordinated frequency controller in Scenario 2 is given as follows:

$$\text{Scenario 2} \quad \tilde{\boldsymbol{P}}_{\rm ref} = \begin{bmatrix} \tilde{P}_{\rm gref1} \\ \tilde{P}_{\rm gref2} \\ \tilde{P}_{\rm gref3} \\ \tilde{P}_{\rm gref4} \\ \tilde{P}_{\rm gref5} \\ \tilde{P}_{\rm gref6} \\ \tilde{P}_{\rm gref8} \\ \tilde{P}_{\rm wref1} \\ \tilde{P}_{\rm wref2} \end{bmatrix} = \begin{bmatrix} 0 \\ 0 \\ 0 \\ 0 \\ 0 \\ 0 \\ 0 \\ -6.72 \\ -6.72 \end{bmatrix} \Delta f + \begin{bmatrix} 0.043 \\ 0.043 \\ 0.064 \\ 0.064 \\ 0.128 \\ 0.128 \\ 0.149 \\ 0.4 \\ 0.4 \end{bmatrix}$$

The simulation results in Fig. 11 have indicated that the proposed frequency controllers are effective in high wind speed scenarios. Compared with the PI controllers, the coordinated frequency controllers demonstrated satisfactory dynamic performance in terms of frequency recovery and reserve active power distribution.

With the help of the proposed frequency controllers, the frequency is able to be restored to its normal value when the emergency occurs. Since the wind speed $V_{\rm w}$ is higher than $V_{\rm rate}$, the rotor speed reaches its limit. This means that DFIGs cannot provide active power reserve by lowering the rotor speed. Therefore, the frequency regulation from DFIGs is realized by adjusting pitch angles. When the pitch angle is decreasing from 14.5° to 11.0° (see Fig. 11(d)), the total output power of DFIGs increases 0.8 p.u., as shown in Fig. 11(c).

Case 3: Medium wind speed ($V_{\rm RSC\text{-}lim} \le V_{\rm w} < V_{rate}$)

In this case, we simulate the scenarios with medium and high wind speeds to further demonstrate the effectiveness of the coordinated frequency controller (27). To make the results comparable, the medium and high wind speeds are constant in Case 3 and the same for DFIGs in each scenario. We consider two scenarios with different wind speeds and initial working states of DFIGs.

Scenario 1:

medium wind speed, $V_{\rm w1} = 10.2$ m/s, with $\theta_{j,0} = 3.7°$.

Scenario 2:

high wind speed, $V_{\rm w2} = 15$ m/s, with $\theta_{j,0} = 14.3°$.

The initial output powers of generators and DFIGs in two scenarios are given in Table X.

TABLE VIII
OUTPUT POWER OF GENERATORS AND DFIGS IN CASE 2

G1/G2	G3/G4	G5/G6	G7/G8	W1/W2
40.6 MW	60.8 MW	1217 MW	141.9 MW	360 MW

TABLE IX
THE TWO OPERATING SCENARIOS IN CASE 2

Scenario 1	PI control scheme for generators and DFIGs
Scenario 2	coordinated frequency control scheme (27) set $P_{{\rm wm}j}(k_{{\rm pd}j}\Delta P_D) - P_{{\rm we}j,0} = \Delta P_{\rm wjmax}$ $(j = 1, 2)$

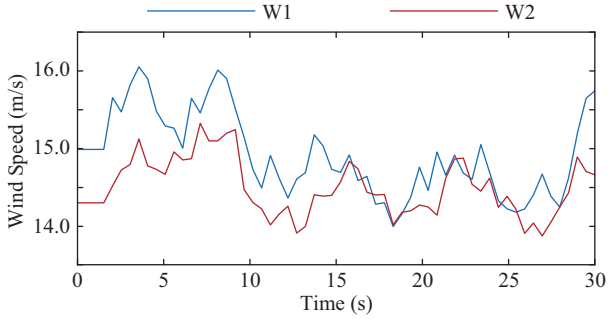

Fig. 10. The wind speed fluctuations in Case 2.

TABLE X
OUTPUT POWER OF GENERATORS AND DFIGS IN CASE 3

Scenario	G1/G2	G3/G4	G5/G6	G7/G8	W1/W2
Scenario 1	44.1 MW	66.2 MW	132.3 MW	154.4 MW	328.1 MW
Scenario 2	40.6 MW	60.8 MW	121.7 MW	141.9 MW	360 MW

The maximal value of reserve power from each DFIG in Scenario 1 and Scenario 2 are 0.364 p.u. and 0.4 p.u., respectively. We consider the same emergency (i.e., G7 drops out at $t = 2$ s). From Table VII, the power imbalances in Scenario 1 and Scenario 2 are 1.544 p.u. and 1.419 p.u.,

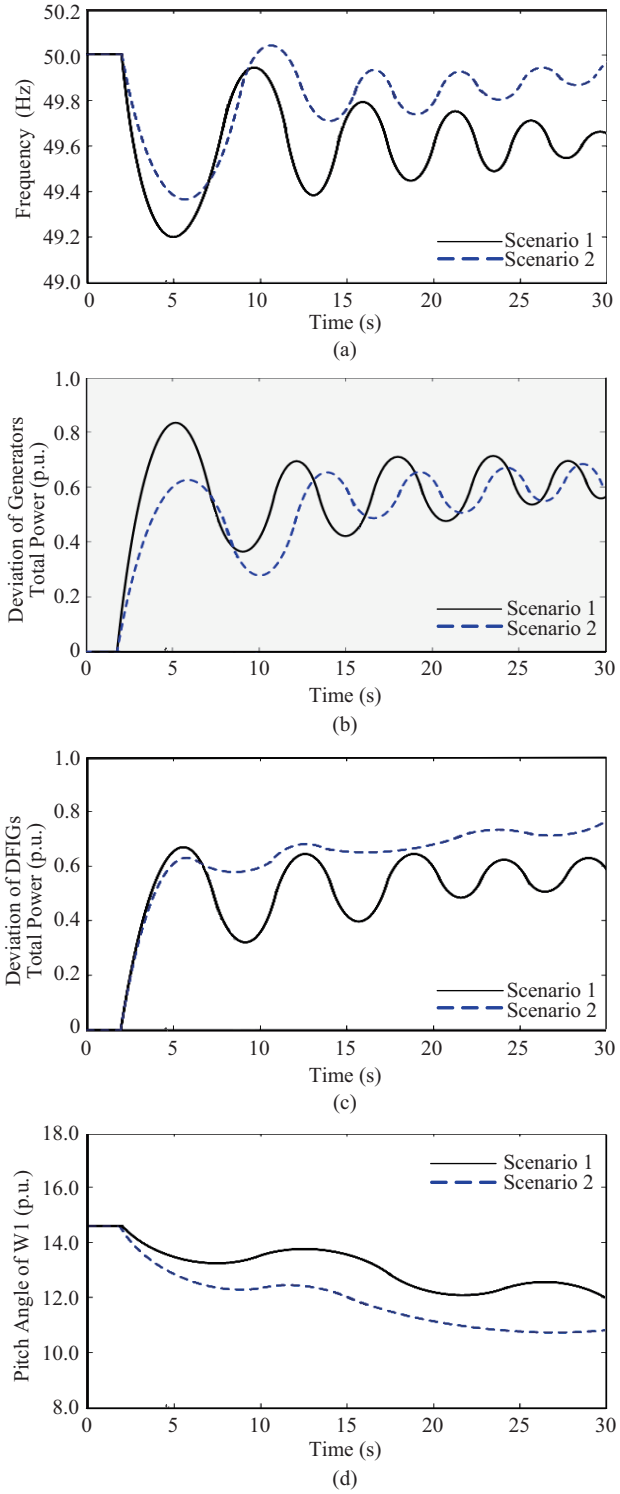

Fig. 11. Simulation results of two scenarios in Case 2. (a) Isolated power system frequency. (b) Total active power deviation of generators. (c) Total active power deviation of DFIGs. (d) Pitch angle of W1.

respectively. Using the ILMI method, one can obtain the feedback controller gains as follows. In Scenario 1, $k_{\mathrm{w1}} = k_{\mathrm{w2}} = -6.49$. In Scenario 2, $k_{\mathrm{w1}} = k_{\mathrm{w2}} = -6.72$. The results in Case 1 have indicated that the power system has a better performance in terms of frequency regulation when DFIGs provide reserve power. In order to get a fast frequency recovery, we select appropriate values of $\tilde{k}_{\mathrm{pd}j}$ in Case 3 such that each DFIG provides reserve power to its maximum. The reserve power from generators is distributed in proportion to installed capacity. The coordinated frequency controllers in two scenarios are given in Table XI.

TABLE XI
THE COORDINATED FREQUENCY CONTROLLERS IN CASE 3

Scenario 1	$\tilde{\boldsymbol{P}}_{\mathrm{ref}} =$	$\begin{bmatrix} \tilde{P}_{\mathrm{gref1}} \\ \tilde{P}_{\mathrm{gref2}} \\ \tilde{P}_{\mathrm{gref3}} \\ \tilde{P}_{\mathrm{gref4}} \\ \tilde{P}_{\mathrm{gref5}} \\ \tilde{P}_{\mathrm{gref6}} \\ \tilde{P}_{\mathrm{gref8}} \\ \tilde{P}_{\mathrm{wref1}} \\ \tilde{P}_{\mathrm{wref2}} \end{bmatrix}$	$=$	$\begin{bmatrix} 0 \\ 0 \\ 0 \\ 0 \\ 0 \\ 0 \\ 0 \\ -6.49 \\ -6.49 \end{bmatrix}$	$\Delta f +$	$\begin{bmatrix} 0.056 \\ 0.056 \\ 0.084 \\ 0.084 \\ 0.169 \\ 0.169 \\ 0.197 \\ 0.364 \\ 0.364 \end{bmatrix}$
Scenario 2	$\tilde{\boldsymbol{P}}_{\mathrm{ref}} =$	$\begin{bmatrix} \tilde{P}_{\mathrm{gref1}} \\ \tilde{P}_{\mathrm{gref2}} \\ \tilde{P}_{\mathrm{gref3}} \\ \tilde{P}_{\mathrm{gref4}} \\ \tilde{P}_{\mathrm{gref5}} \\ \tilde{P}_{\mathrm{gref6}} \\ \tilde{P}_{\mathrm{gref8}} \\ \tilde{P}_{\mathrm{wref1}} \\ \tilde{P}_{\mathrm{wref2}} \end{bmatrix}$	$=$	$\begin{bmatrix} 0 \\ 0 \\ 0 \\ 0 \\ 0 \\ 0 \\ 0 \\ -6.72 \\ -6.72 \end{bmatrix}$	$\Delta f +$	$\begin{bmatrix} 0.043 \\ 0.043 \\ 0.064 \\ 0.064 \\ 0.128 \\ 0.128 \\ 0.149 \\ 0.4 \\ 0.4 \end{bmatrix}$

As shown in Fig. 12(a), with the help of the proposed frequency controllers, the frequency is able to restore to its normal value when the emergency occurs in two scenarios. In Scenario 1, the wind speed V_{w1} is lower than the rated wind speed V_{rate}, which means RSC (see Fig. 12(d)) and PAC (see Fig. 12(e)) are activated for frequency regulation. The rotor speed decreases about 0.027 p.u. and the pitch angle drops from the initial value (3.7°) to about 0°. In Scenario 2, since V_{w2} is higher than V_{rate}, the rotor speed reaches its limit. This means that DFIGs cannot provide active power reserve by lowering the rotor speed. Therefore, the frequency regulation from DFIGs is realized by adjusting pitch angles. When the pitch angle decreases from 14.3° to 11.0°, the total output power of the DFIGs increases 0.8 p.u., as shown in Fig. 12(c).

The simulation results indicate that the coordinated frequency controller (27) are also effective for medium wind speeds scenarios.

VI. CONCLUSION

This paper has investigated the emergency frequency control problems in an actual isolated power system with high penetration of wind power. Observing that DFIGs are capable of providing active power reserve for frequency regulation via RSC and PAC, we have developed coordinated frequency control schemes for an isolated power grid that is composed of generators and DFIGs. Because of the nonlinearity of wind power, emergency frequency control is formulated as a nonlinear regulator problem. With the help of nonlinear regulator theory, a frequency controller for a simple power system with single generator and single DFIG was first designed. The coordinated frequency controllers for the isolated power system under various wind speeds were then derived based on the controllers obtained for the simple power system. Simulation studies have

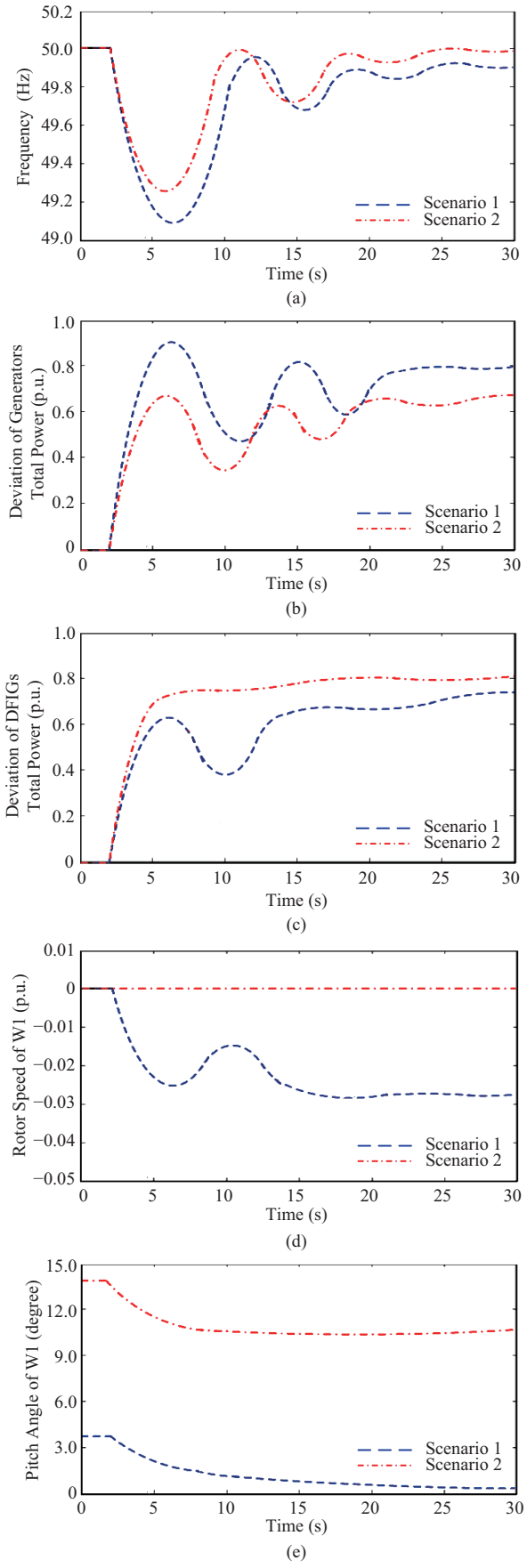

Fig. 12. Simulation results of two scenarios in Case 3. (a) Isolated power system frequency. (b) Total active power deviation of generators. (c) Total active power deviation of DFIGs. (d) Pitch angle of W1.

demonstrated the effectiveness and robustness of the proposed nonlinear frequency control schemes in restoring frequency to the normal range in the presence of large active power imbalances. Compared with the performance of PI controllers, the proposed coordinated frequency controllers exhibit more satisfactory dynamic performance in both low and high wind speed scenarios, even when wind speed fluctuations exist. However, for the variable wind speeds, the power system frequency still fluctuates because the coordinated frequency controllers are only calculated by the time that the power imbalance occurs. The output power of DFIGs is not constant during the frequency response process, leading to the frequency fluctuations. For the next study, an online coordinated frequency controller design method will be studied to update the controller in period, which will improve the robustness against wind speed.

The frequency control method based on the regulator theory is also applicable to demand side regulation in microgrids. Future studies will focus on studying flexible loads and coordinating the generation side and demand side control.

APPENDIX

Tables AI and AII list the PI controller parameters of thermal generators and DFIGs in Case1 and Case 2, respectively.

TABLE AI
PI CONTROLLER PARAMETERS OF GENERATORS AND DFIGS IN CASE1

Generator/DFIG	G1/G2	G3/G4	G5/G6	G7/G8	W1/W2
K_P	5.0	5.0	6.0	6.0	10
K_I	0.3	0.3	0.5	0.5	0.4

TABLE AII
PI CONTROLLER PARAMETERS OF GENERATORS AND DFIGS IN CASE 2

Generator/DFIG	G1/G2	G3/G4	G5/G6	G7/G8	W1/W2
K_P	5.0	5.0	6.0	6.0	15
K_I	0.3	0.3	0.5	0.5	0.1

REFERENCES

[1] China Electricity Council, "China's power industry development annual report 2021," China Electricity Council, China, Report, Jul. 2021.
[2] J. Lin, Y. Z. Sun, Y. H. Song, W. Z. Gao, and P. Sorensen, "Wind power fluctuation smoothing controller based on risk assessment of grid frequency deviation in an isolated system," *IEEE Transactions on Sustainable Energy*, vol. 4, no. 2, pp. 379–392, Apr. 2013.
[3] N. Hatziargyriou, I. Margaris, I. Stavropoulou, S. Papathanassiou, and A. Dimeas, "Noninterconnected island systems: the Greek case," *IEEE Electrification Magazine*, vol. 5, no. 2, pp. 17–27, Jun. 2017.
[4] J. Østergaard and J. E. Nielsen, "The bornholm power system - an overview," Centre for Electric Technology, Technical University of Denmark, Jan. 2008.
[5] O. Weiss, D. Bogdanov, K. Salovaara, and S. Honkapuro, "Market designs for a 100% renewable energy system: Case isolated power system of Israel," *Energy*, vol. 119, pp. 266–277, Jan. 2017.
[6] X. L. Liu, Y. B. Liu, J. Y. Liu, Y. Xiang, and X. D. Yuan., "Optimal planning of AC-DC hybrid transmission and distributed energy resource system: Review and prospects," *CSEE Journal of Power and Energy Systems*, vol. 5, no. 3, pp. 409–422, Sep. 2019.
[7] B. Mohandes, M. S. E. Moursi, N. Hatziargyriou, and S. E. Khatib., "A review of power system flexibility with high penetration of renewables," *IEEE Transactions on Power Systems*, vol. 34, no. 4, pp. 3140–3155, Jul. 2019.

[8] Y. Bao, J. Xu, S. Y. Liao, Y. Z. Sun, X. Li, Y. Z. Jiang, D. P. Ke, J. Yang, and X. T. Peng, "Field verification of frequency control by energy-intensive loads for isolated power systems with high penetration of wind power," *IEEE Transactions on Power Systems*, vol. 33, no. 6, pp. 6098–6108, Nov. 2018.

[9] H. Jiang, J. Lin, Y. H. Song, W. Z. Gao, Y. Xu, B. Shu, X. M. Li, and J. X. Dong, "Demand side frequency control scheme in an isolated wind power system for industrial aluminum smelting production," *IEEE Transactions on Power Systems*, vol. 29, no. 2, pp. 844–853, Mar. 2014.

[10] J. Xu, S. Y. Liao, Y. Z. Sun, X. Y. Ma, W. Z. Gao, X. M. Li, J. H. Gu, J. X. Dong, M. Zhou, "An isolated industrial power system driven by wind-coal power for aluminum productions: a case study of frequency control," *IEEE Transactions on Power Systems*, vol. 30, no. 1, pp. 471–483, Jan. 2015.

[11] R. Dhua, D. Chatterjee, and S. K. Goswami, "Study of improved load sharing methodologies for distributed generation units connected in a microgrid," *CSEE Journal of Power and Energy Systems*, vol. 3, no. 3, pp. 311–320, Sep. 2017.

[12] J. Li, S. Chen, X. Y. Wang, and T. J. Pu, "Load shedding control strategy in power grid emergency state based on deep reinforcement learning," *CSEE Journal of Power and Energy Systems*, vol. 8, no. 4, pp. 1175–1182, 2022.

[13] Y. S. Sun, Z. X. Zhao, M. Yang, D. Q. Jia, W. Pei, and B. Xu, "Overview of energy storage in renewable energy power fluctuation mitigation," *CSEE Journal of Power and Energy Systems*, vol. 6, no. 1, pp. 160–173, Mar. 2020.

[14] M. X. Han, G. T. Bitew, S. A. Mekonnen and W. L. Yan, "Wind power fluctuation compensation by variable speed pumped storage plants in grid integrated system: Frequency spectrum analysis," *CSEE Journal of Power and Energy Systems*, vol. 7, no. 2, pp. 381–395, Mar. 2021.

[15] R. Pena, J. C. Clare, and G. M. Asher, "Doubly fed induction generator using back-to-back PWM converters and its application to variable-speed wind-energy generation," *IEE Proceedings-Electric Power Applications*, vol. 143, no. 3, pp. 231–241, May 1996.

[16] M. Sun, Y. Min, L. Chen, K. Y. Hou, D. M. Xia and H. Y. Mao, "Optimal auxiliary frequency control of wind turbine generators and coordination with synchronous generators," *CSEE Journal of Power and Energy Systems*, vol. 7, no. 1, pp. 78–85, Jan. 2021.

[17] F. Teng and G. Strbac, "Assessment of the role and value of frequency response support from wind plants," *IEEE Transactions on Sustainable Energy,* vol. 7, no. 2, pp. 586–595, Apr. 2016.

[18] E. Muljadi, V. Gevorgian, M. Singh, and S. Santoso, "Understanding inertial and frequency response of wind power plants," in *Proceedings of 2012 IEEE Power Electronics and Machines in Wind Applications*, Denver, CO, USA, 2012, pp. 1–8.

[19] G. Y. Xu, F. L. Liu, J. X. Hu, and T. S. Bi, "Coordination of wind turbines and synchronous generators for system frequency control," *Renewable Energy*, vol. 129, pp. 225–236, Dec. 2018.

[20] I. D. Margaris, S. A. Papathanassiou, N. D. Hatziargyriou, A. D. Hansen, and P. Sorensen, "Frequency control in autonomous power systems with high wind power penetration," *IEEE Transactions on Sustainable Energy*, vol. 3, no. 2, pp. 189–199, Apr. 2012.

[21] J. J. Zhao, X. Lyu, Y. Fu, X. G. Hu and F. X. Li, "Coordinated microgrid frequency regulation based on DFIG variable coefficient using virtual inertia and primary frequency control," *IEEE Transactions on Energy Conversion*, vol. 31, no. 3, pp. 833–845, Sep. 2016.

[22] H. C. Luo, Z. C. Hu, H. C. Zhang, and H. M. Chen, "Coordinated active power control strategy for deloaded wind turbines to improve regulation performance in AGC," *IEEE Transactions on Power Systems*, vol. 34, no. 1, pp. 98–108, Jan. 2019.

[23] J. Pahasa and I. Ngamroo, "Coordinated control of wind turbine blade pitch angle and PHEVS using MPCS for load frequency control of microgrid," *IEEE Systems Journal*, vol. 10, no. 1, pp. 97–105, Mar. 2016.

[24] X. B. Kong, X. J. Liu, L. L. Ma, and K. Y. Lee, "Hierarchical distributed model predictive control of standalone wind/solar/battery power system," *IEEE Transactions on Systems, Man, and Cybernetics: Systems*, vol. 49, no. 8, pp. 1570–1581, Aug. 2019.

[25] Y. G. Du, J. Wu, S. Y. Li, C. N. Lo, and I. C. Paschalidis, "Distributed MPC for coordinated energy efficiency utilization in microgrid systems," *IEEE Transactions on Smart Grid*, vol. 10, no. 2, pp. 1781–1790, Mar. 2019.

[26] T. Cui, W. Lin, Y. Z. Sun, J. Xu, and H. K. Zhang, "Excitation voltage control for emergency frequency regulation of Island power systems with voltage dependent loads," *IEEE Transactions on Power Systems*, vol. 31, no. 2, pp. 1204–1217, Mar. 2016.

[27] C. Zhang, W. Lin, D. P. Ke, and Y. Z. Sun, "Smoothing tie-line power fluctuations for industrial Microgrids by demand side control: an output regulation approach," *IEEE Transactions on Power Systems*, vol. 34, no. 5, pp. 3716–3728, Sep. 2019.

[28] Y. Z. Sun, J. Lin, Y. H. Song, J. Xu, X. M. Li, and J. X. Dong, "An industrial system powered by wind and coal for aluminum production: A case study of technical demonstration and economic feasibility," Energies, vol. 5, no. 11, pp. 4844–4869, Nov. 2012.

[29] P. M. Anderson and M. Mirheydar, "A low-order system frequency response model," IEEE Transactions on Power Systems, vol. 5, no. 3, pp. 720–729, Aug. 1990.

[30] N. R. Ullah, T. Thiringer, and D. Karlsson, "Temporary primary frequency control support by variable speed wind turbines—potential and applications," *IEEE Transactions on Power Systems*, vol. 23, no. 2, pp. 601–612, May 2008.

[31] K. V. Vidyanandan and N. Senroy, "Primary frequency regulation by deloaded wind turbines using variable droop," *IEEE Transactions on Power Systems*, vol. 28, no. 2, pp. 837–846, May 2013.

[32] L. R. Chang-Chien, C. C. Sun, and Y. J. Yeh, "Modeling of wind farm participation in AGC," *IEEE Transactions on Power Systems*, vol. 29, no. 3, pp. 1204–1211, May 2014.

[33] A. B. T. Attya and T. Hartkopf, "Control and quantification of kinetic energy released by wind farms during power system frequency drops," *IET Renewable Power Generation*, vol. 7, no. 3, pp. 210–224, May 2013.

[34] L. M. Fernández, F. Jurado, and J. R. Saenz, "Aggregated dynamic model for wind farms with doubly fed induction generator wind turbines," *Renewable Energy*, vol. 33, no. 1, pp. 129–140, Jan. 2008.

[35] S. Heier, *Grid Integration of Wind Energy*, G. Roth, R. Waddington, trans, 3rd ed., New York: John Wiley & Sons, Ltd, 2014.

[36] H. T. Ma and B. H. Chowdhury, "Working towards frequency regulation with wind plants: combined control approaches," *IET Renewable Power Generation*, vol. 4, no. 4, pp. 308–316, Jul. 2010.

[37] A. Isidori and C. I. Byrnes, "Output regulation of nonlinear systems," *IEEE Transactions on Automatic Control*, vol. 35, no. 2, pp. 131–140, Feb. 1990.

[38] M. E. Aggoune, F. Boudjemaa, A. Bensenouci, A. Hellal, M. R. Elmesai, and S. V. Vadari, "Design of variable structure voltage regulator using pole assignment technique," *IEEE Transactions on Automatic Control*, vol. 39, no. 10, pp. 2106–2110, Oct. 1994.

[39] Y. He and Q. G. Wang, "An improved ILMI method for static output feedback control with application to multivariable PID control," *IEEE Transactions on Automatic Control*, vol. 51, no. 10, pp. 1678–1683, Oct. 2006.

[40] S. Sönmez and S. Ayasun, "Stability region in the parameter space of PI controller for a single-area load frequency control system with time delay," *IEEE Transactions on Power Systems*, vol. 31, no. 1, pp. 829–830, Jan. 2016.

[41] L. Jiang, W. Yao, Q. H. Wu, J. Y. Wen, and S. J. Cheng, "Delay-dependent stability for load frequency control with constant and time-varying delays," *IEEE Transactions on Power Systems*, vol. 27, no. 2, pp. 932–941, May 2012.

[42] W. Lin, Z. T. Lu, and W. Wei, "Asymptotic tracking control for wind turbines in variable speed mode," *IEEE/CAA Journal of Automatica Sinica*, vol. 4, no. 3, pp. 569–576, Jul. 2017.

[43] W. Lin and L. Y. Dai, "Solutions to the output regulation problem of linear singular systems," *Automaticam*, vol. 32, no. 12, pp. 1713–1718, Dec. 1996.

Xin Ding received the B.S. degree in Electrical Engineering and Automation from the Shanghai University of Electrical Power, Shanghai, China, in 2014, and the Ph.D. degree in Power Engineering from Wuhan University, Wuhan, China, in 2022. He is now a Research Associate at University of Shanghai for Science and Technology. His research interests include operation and analysis of power system with renewable energy and load control.

Wei Lin received the B.S. degree in Electrical Engineering from the Dalian University of Science and Technology in 1983, the M.S. degree in Electrical Engineering from the Huazhong University of Science and Technology in 1986, and the D.Sc. and M.S. degrees in Systems Science and Mathematics from Washington University, St. Louis, MO, USA, in 1993 and 1991, respectively. Since Spring 1996, he has been a Professor with the Department of Electrical Engineering and Computer Science, Case Western Reserve University, Cleveland, OH, USA. His research interests include nonlinear control, time-delay systems, homogeneous systems theory, estimation and adaptive control, under-actuated mechanical and biologically-inspired systems, renewable energy, power systems, and smart grids.

Jian Xu received the B.S. and Ph.D. degrees in Electrical Engineering from Wuhan University, Wuhan, China, in 2002 and 2007, respectively. He is currently a Professor with the School of Electrical Engineering and Automation, Wuhan University. His research interests include power system operation, voltage stability, and wind power control and integration.

Yuanzhang Sun received the B.S. degree from the Wuhan University of Hydro and Electrical Engineering, Wuhan, China, in 1987, the M.S. degree from Electric Power Research Institute, Beijing, China, in 1982, and the Ph.D. degree in Electrical Engineering from Tsinghua University, Beijing, in 1988. He is currently a Professor with the School of Electrical Engineering with Wuhan University, and the Chair Professor with the Department of Electrical Engineering and the Vice Director of the State Key Lab of Power System Control and Simulation, Tsinghua University. His main research interests include the areas of power system dynamics and control, wind power, voltage stability and control, and reliability.

Liangzhong Yao is the Director of Smart Grid Research Institute, and the Professor in the School of Electrical Engineering and Automation at Wuhan University, China. He is the Member of Academia Europaea, Fellow of IEEE, Fellow of IET, and Fellow of AAIA. Prior to joining Wuhan University in 2018, he was the Vice President and Honorary Chief Engineer at China Electric Power Research Institute (2012–2018), the Vice President at State Grid Electric Power Research Institute (2011–2012), the Department Head and Senior Expert at Alstom Grid Research &Technology Centre in the UK (2004–2011), the Senior Power System Analyst at ABB UK Ltd (1999–2004), the Postdoctoral Research Associate at the University of Manchester (1995–1999), and the Postdoctoral Research Fellow and Associate Research Professor at Tsinghua University (1993–1995), respectively. His research fields cover renewable energy grid integration and control, energy storage grid integration and control, power electronics converter control, and HVDC and DC grid technologies, etc.

Beilin Mao is the Associate Research Professor in the School of Electrical Engineering and Automation at Wuhan University, China. She received the Ph.D. degree in Electrical Power Engineering from the University of Bath in the UK in 2000. She is the member of IET and CIGRE, and the UK Chartered Engineer. Prior to joining Wuhan University in 2020, she was the Senior Power System Consultant and Senior Protection Engineer for HV Smart Substation at ABB UK Ltd from 2000 to 2020, Associate Research Professor in the Institute of Nuclear and New Energy Technology at Tsinghua University from 1993 to 1996, and Senior Electrical Engineer at Xinjiang Water Conservancy Power Research Institute from 1983 to 1993, respectively. Her research fields cover power system analysis, power system protection and control, smart substation design, renewable energy grid integration and control, etc.